From the Department of Clinical Neuroscience, Psychiatry Section
Karolinska Institutet, Stockholm, Sweden

DEVELOPMENT, VALIDATION AND APPLICATION OF ADVANCED NEUROIMAGING ANALYSIS TOOLS FOR IN VIVO NEURORECEPTOR STUDIES

Zsolt Cselényi

Stockholm 2005

Cover illustration:
Volume rendering of dopamine D_2-receptor binding potential created with 3-D wavelet-aided parametric imaging. Left column: right side views; right colum: left side views. First row: posterolateral views; second row: lateral views; third row: anterolateral views. Lowest binding potential regions are completely or almost completely transparent. Besides, for ease of visualization, only certain ranges of binding potential are set to partially opaque, all other values were assigned complete transparency. Visible ranges: around 0.1, transparent blue (majority of the cortex, especially the occipital, the parietal and the frontal cortices); around 0.7, cyan (the temporal cortex, the anterior cingulate cortex, outer parts of the thalamus and the hypophysis); around 1.5, green (inferior, internal parts of the temporal cortex, intermediate boundaries of thalamus, internal parts of the hypophysis); 3.0 and up, yellow, red, white (internal parts of the thalamus, the striatum).

Printed by the generous support of Gedeon Richter Ltd., Budapest, Hungary

Published and printed by Gedeon Richter Ltd.
Budapest, Hungary

ISBN 91-7140-261-6

Even he, to whom most things that most people would think were pretty smart were pretty dumb, thought it was pretty smart
The Salmon of Doubt – Douglas Adams (*1952-2001*)

To Veronika

ABSTRACT

Positron emission tomography (PET) is an imaging technology, which can be used to study neuroreceptors in the human brain in vivo. The technique estimates the regional binding of radiolabelled ligands to neuroreceptors and the data are commonly displayed as images showing the distribution of radioactivity in the brain volume. A traditional image analysis approach builds upon reduction of noise in a region of interest (ROI) by averaging radioactivity in the volume elements (voxels) of the ROI. This approach is efficient to improve the reliability of the time curves but does not allow for a detailed analysis of the entire brain. To obtain detailed three-dimensional maps of binding parameters in brain, novel approaches have been developed during recent years.

The aim of the present thesis project is to examine and validate the repertoire of advanced computerised tools used to obtain parametric maps of receptor binding in basic and clinical neuroscience research. In addition, the increasing number of suitable PET radioligands, targeted for different neuroreceptor systems, calls for approaches that allow for a combined analysis of multiple receptor systems.

A parametric mapping approach using wavelet filtering was evaluated in a cross-validation design. Data from PET-studies on regional D_2/D_3 dopamine and 5-HT_{1A} serotonin receptor binding in the human brain were used to compare the binding potential (BP) estimates of the wavelet-based approach and other parametric imaging approaches to the ROI-based graphical Logan analysis which was used as a reference. The approach using three-dimensional wavelet filtering was noise-tolerant and yielded BP maps with regional averages closely matching the reference values. Overall, the wavelet-based approach seemed to provide the most valid and reliable estimates across regions with a wide range of receptor densities. However, there was some loss of resolution, which may be critical for analysis of binding in small anatomical regions.

Another set of parametric mapping approaches is similar to the ROI-based analyses in the sense that signal averaging is used to reduce noise. However, these approaches do not average the time-activity curves (TAC's) of spatially adjacent voxels but that of voxels having a TAC with a similar shape. A process was developed to classify voxels into a large number of groups (clusters) and thus to obtain an average TAC for voxels with a similar TAC. The classification was performed using an artificial neural network model, called the "growing adaptive neural gas" (GANG), which was developed as part of the thesis. Parameter estimation was performed on the average TAC's and the parameters were then back-projected to the original spatial locations of the voxels thereby providing 3D parametric maps. The approach was applied to PET images measuring D_2/D_3 receptor binding. The results indicate that the approach can be used to effectively reduce noise. The created parametric maps were highly detailed and the binding distribution was consistent with parametric images obtained with previous approaches.

Novel technical approaches are required in combined analyses of multiple neuroreceptor systems. Such approaches have to be capable of operating on very large parametric image datasets. An initial step is the development of exploratory data-mining tools, which provide guidance as to the "structure" of complex multi-individual, multi-receptor datasets. For this task, an unsupervised and unbiased data-mining tool was developed and proposed. The tool includes a GANG-based clustering of multi-receptor data. The proposed approach was tested on a dataset containing BP maps of the serotonin transporter and the 5-HT_{1A} receptors obtained in the same individuals. The outputs of the method were multi-receptor maps with potential to reveal complex relationships and tendencies in a dataset with several ligands. Such maps may have value in clinical research on multi-receptor interactions and pattern changes in the human brain.

In conclusion, the present thesis has examined and extended a methodological platform that allows for additional gain of information from routinely generated data in PET studies on neuroreceptor binding. The results support application of parametric image analysis in basic and clinical research.

LIST OF PUBLICATIONS

I. Cselényi Z, Olsson H, Farde L, Gulyás B. (2002) Wavelet-aided parametric mapping of cerebral dopamine D_2 receptors using the high affinity PET radioligand [^{11}C]FLB 457. *NeuroImage*, **17**:47-60.

II. Cselényi Z, Olsson H, Halldin C., Gulyás B., Farde L. (2005) A comparison of recent parametric neuroreceptor mapping approaches based on measurements with the high affinity PET radioligands [^{11}C]FLB 457 and [^{11}C]WAY100635. *Submitted to NeuroImage*

III. Cselényi, Z. (2005) Mapping the dimensionality, density and topology of data: the growing adaptive neural gas. *Computer Methods and Programs in Biomedicine (in press).*

IV. Cselényi Z, Olsson H, Farde L., Halldin C., Gulyás B. (2005) Mapping of binding parameters in the human brain using an artificial neural network approach to reduce the noise effect. *Manuscript.*

V. Cselényi Z, Lundberg J, Halldin C, Farde L, Gulyás B. (2004) Joint explorative analysis of neuroreceptor subsystems in the human brain: application to receptor-transporter correlation using PET data. *Neurochem Int.* **45**:773-81.

CONTENTS

LIST OF ABBREVIATIONS

CNS	Central nervous system
SPECT	Single-photon emission computed tomography
PET	Positron emission tomography
BP	Binding potential
TAC	Time-(radio)activity curve
SRTM	Simplified reference tissue model
LSRTM	Linearised simplified reference tissue model
DV_{tot}	Total distribution volume
DVR	Distribution volume ratio
ROI	Region of interest
WT	Wavelet transform
DWT	Dyadic wavelet transform
3DWT	3-dimensional wavelet transform
2DTI	2-dimensional translation-invariant (wavelet transform)
BFM	Basis function method
FDG	Fluoro-desoxyglucose
UCA	Unsupervised cluster analysis
ANN	Artificial neural network
SOM	Self-organizing map
GANG	Growing adaptive neural gas
GNG	Growing neural gas
RF	Receptive field
DEPICT	Data-driven estimation of parametric images based on compartmental theory
HBA	Human Brain Atlas

1 INTRODUCTION

Positron emission tomography (PET) is an imaging modality used to study brain metabolism and neurotransmission systems in experimental animals and human subjects. Neuronal membrane bound receptor proteins and transport proteins are major biological targets in most such studies. Understanding the role of neuroreceptors in relation to brain function has proven to be of scientific as well as clinical value. However, extraction of reliable and anatomically detailed information on neuroreceptor binding from PET images poses challenges since PET measurements are sensitive to various biological and physical factors. The development of advanced neuroimaging analysis tools may thus provide added value in analyses of neuroreceptor binding in the human brain.

The human brain contains about seven hundred different neuroreceptors of which three hundred belongs to the olfactory system (Siegel et al., 1999; Cooper et al., 2002). They are most commonly defined by the chemical composition of their specific neurotransmitter. Neurons expressing specific types of neuroreceptor proteins display a characteristic pattern of distribution both at macroscopic and microscopic level. The morphological patterns are thought to be a lead to understand the functional significance. Therefore the notion of neuroreceptor systems and subsystems referring to morpho-functional entities in the CNS has been introduced. A system consists of specific neural pathways and neuron populations expressing a given neuroreceptor type or subtype.. Neuroreceptor studies in basic as well as clinical research seek to explain physiological and pathological conditions in terms of the involvement of different neuroreceptor systems. In particular, such studies claim to offer the following benefits:

- Insight into the involvement of different neuroreceptor systems in higher level functioning of the brain such as motor, sensory functions or cognition.
- Understanding of the inter-individual variability of the human brain through the mapping of receptor distribution in relation to genetic and environmental factors.
- Contribution to the understanding of neuro-psychiatric disorders by detailed brain mapping in relation to pathological conditions.
- Discovery and control of pharmacological interventions, i.e. development and testing of drugs acting on certain neuroreceptor systems or subsystems.

The present thesis work aimed at establishing a methodological platform to support neuroreceptor research in the areas listed above. Specifically, the methodologies in the focus of the thesis can be positioned according to the following two levels:

- First level: calculation of images characterising ligand binding from the raw experimental data.
- Second level: creation of images showing relationships between different neuroreceptor systems or subsystems or between neuroreceptor systems and various physiological or pathological conditions.

The following discussion is structured according to these levels of neuroreceptor studies.

1.1 FIRST LEVEL OF NEURORECEPTOR STUDIES

Imaging of neuroreceptors *in vivo* can be achieved using single-photon emission computed tomography (SPECT) or positron emission tomography (PET) (English and Brown, 1990; Verhoeff, 1993; Carson et al., 1998). Both build upon a similar approach: a solution, containing the radioligand, is injected intravenously and the emitted radioactivity is detected using rings of detectors around the head. The radioligands bind specifically to the target neuroreceptors. The more advanced of the two techniques is PET allowing higher resolution and absolute quantification. A typical camera today has an intrinsic spatial resolution of 3.6 mm in plain of the detector rings at the centre of the field of view and 4.0 mm axially (e.g. Wienhard et al., 1994). PET is the technique in the focus of the thesis.

As the name implies, PET uses radioligands labelled with positron-emitting radionuclides, such as ^{11}C, ^{18}F, ^{15}O or ^{13}N. The half-life of these radionuclides is relatively short, between 20 to 110 minutes, requiring on site radioligand production, i.e. a cyclotron and a radiochemistry unit. At decay, the emitted positron particle travels a few millimetres in the tissue, the distance depending on the energy of the particle. After that the positron annihilates at a collision with its anti-particle, an electron. The annihilation generates two γ-photons travelling at about 180 degrees to each other.

The γ-ray pairs are detected as coinciding events in the detector rings, which enables high precision of localisation of the annihilation and thus the positron emission event. Modern PET cameras detect coincidence events not only in plane of a detector ring but also those between two different rings. The coincidence events are registered by the PET computer system. After data acquisition the computer reconstructs a three-dimensional image of radioactivity within the volume of acquisition. Quantified radioactivity values are obtained with the help of an attenuation correction that is obtained for each subject by a transmission scan using an external source of γ-photons. A typical reconstructed 3D image consists of around 50 image slices with a matrix size of 128 × 128. Each volume element (voxel) of a PET image has a size of 2.0 × 2.0 mm in plane and 3-4 mm axially. In case of neuroreceptor studies several consecutive 3D images are acquired to obtain information on the temporal change of radioactivity, which is often referred to as time-radioactivity curves (TAC's). The four-dimensional PET images of quantified radioactivity may be viewed as "raw data" for neuroreceptor studies.

The goal of the first level of data processing is the creation of biologically meaningful parameters for receptor binding. However, such processing has to face two major problems:

- PET images for neuroreceptor studies contain radioactivity from ligand molecules in the cerebral blood volume, those unbound and specifically or unspecifically bound in tissue as well as from possible radiolabelled metabolites of the ligand.
- PET images have low physical signal-to-noise ratio for various reasons such as the use of limited amounts of radioactivity, or relatively short periods (few minutes) of data collection within timeframes of image acquisition for neuroreceptor studies.

To circumvent the first problem, mathematical models have been defined, which aspire to describe the pharmacokinetics of radioligand binding in terms of the time-course of blood, more precisely plasma, radioligand concentration. The most widely applied model is the compartmental model, which defines compartments as pools of radioligands in different states relative to the blood-brain barrier and various binding sites (Figure 1) (Carson et al., 1998).

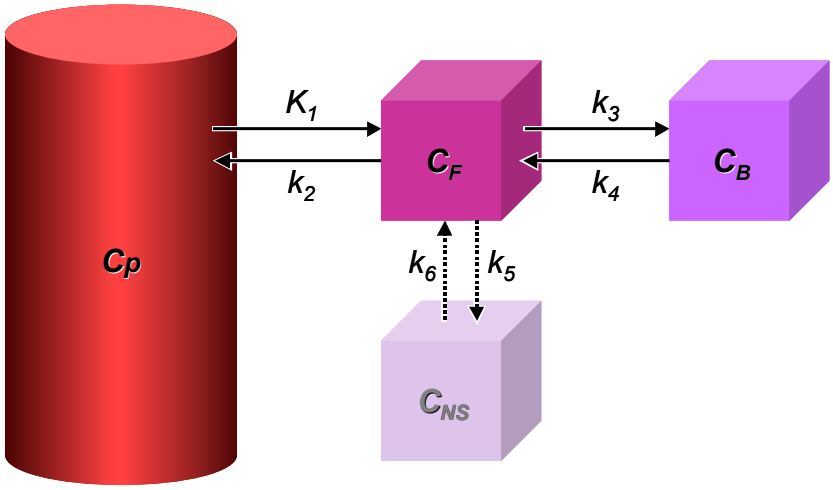

Figure 1

The "force" driving the compartmental model is the input function, i.e. the plasma radioligand pool (C_p). The input compartment is communicating with the free-radioligand compartment in the brain tissue (C_F) through the blood-brain barrier. The pool of radioligand bound to the target receptors (C_B) defines the next compartment, which is in continuous exchange with the free-radioligand compartment through the reversible process of ligand binding. A fourth optional compartment can be identified in case of some radioligands. This encompasses the pool of radioligands bound to any other sites than the target neuroreceptors; a compartment defined as non-specific binding (C_{NS}). The model describes the exchange of radioligand between the compartments in terms of kinetic rate constants defining the bidirectional flux of radioligand from one compartment to another (K_1 - k_6). Thus the rate constants can be assumed to have biological relevance. Furthermore, some derived parameters are of even greater importance for neuroreceptor studies. The most important of these is the ratio of k_3 to k_4, This parameter is referred to as the binding potential (BP), and is the major output parameter of first level neuroreceptor studies. The BP corresponds to the ratio of receptor density (B_{max}) and the binding affinity (K_d) and is thus proportional to the concentration of neuroreceptors available for binding. The rate constants of the compartmental model are obtained via an optimisation process based on a plasma TAC as input and a total tissue TAC as the curve to fit. Therefore, besides acquiring the PET image, the experimental procedure has to include blood sampling to obtain this plasma input function. It must be noted that most radioligands are metabolised *in vivo* and thus the input function must be corrected for metabolites with retained radioactivity. Figure 2 displays characteristic theoretical (noise-free) TAC's for plasma and brain tissues with different amounts of free receptors.

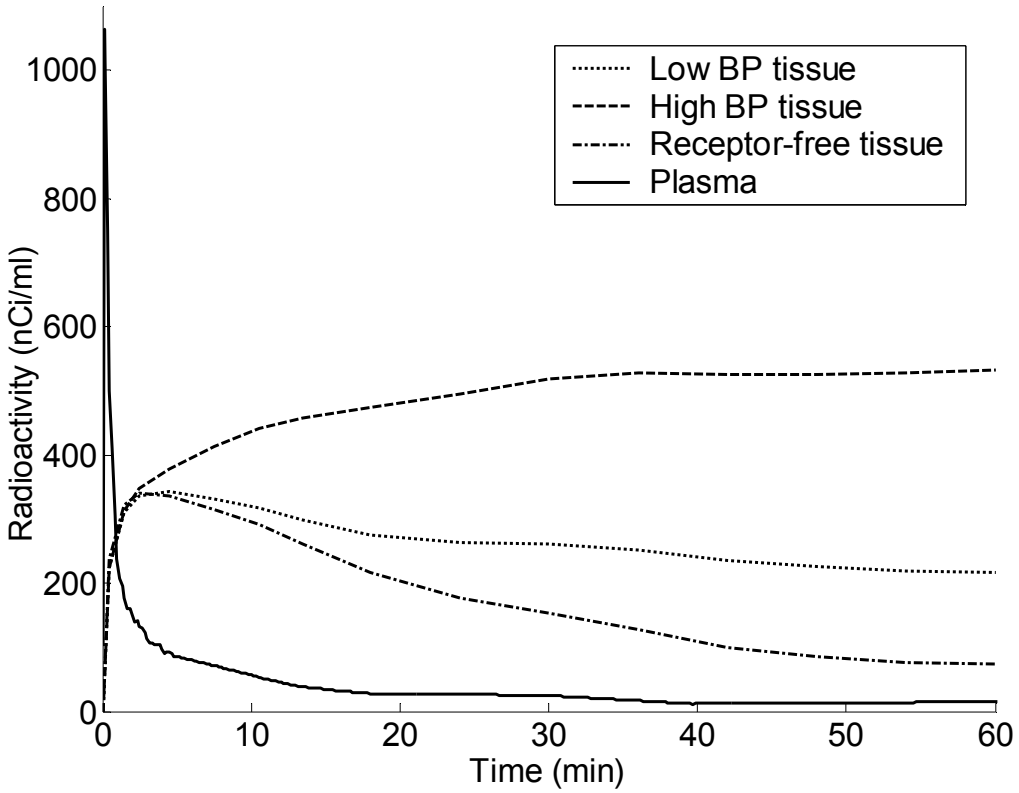

Figure 2

In case where blood sampling is not available, a modified version of the compartmental model can be used. This utilises radioactivity information from a region of the brain that is devoid of the target neuroreceptor known as reference region (dash-dotted line in Figure 2). Accordingly, this is referred to as the reference tissue compartmental model. This model gained popularity because it is less invasive and still enables the calculation of important binding parameters such as BP. Further modifications have been introduced to facilitate convergence by reducing the number of variables to be fitted. This is the simplified reference tissue model (SRTM) (Lammertsma and Hume, 1996). It also has a linearised version (LSRTM) that is useful for the quick calculation of BP (Logan et al., 2001). Another linear fit is Logan's linear graphical approach that can be derived from the compartmental model (Logan et al., 1990; Logan et al., 1996). It has both a plasma input and a reference input version providing the parameters of total distribution volume (DV_{tot}) or distribution volume ratio (DVR), respectively.

Dealing with the second problem, i.e. noise in PET images, has been a major challenge in neuroreceptor studies *in vivo*. TAC's of individual voxels of the four-dimensional PET image have proven to be too noisy for direct fitting of the parameters of the compartmental model. Figure 3 displays sample TAC's of individual voxels in the brain from a PET image obtained using the radioligand [^{11}C]FLB 457, a high affinity dopamine D_2/D_3 receptor antagonist radioligand. In contrast to the curves in Figure 2, these TAC's are noisy, preventing the direct fitting of kinetic parameters.

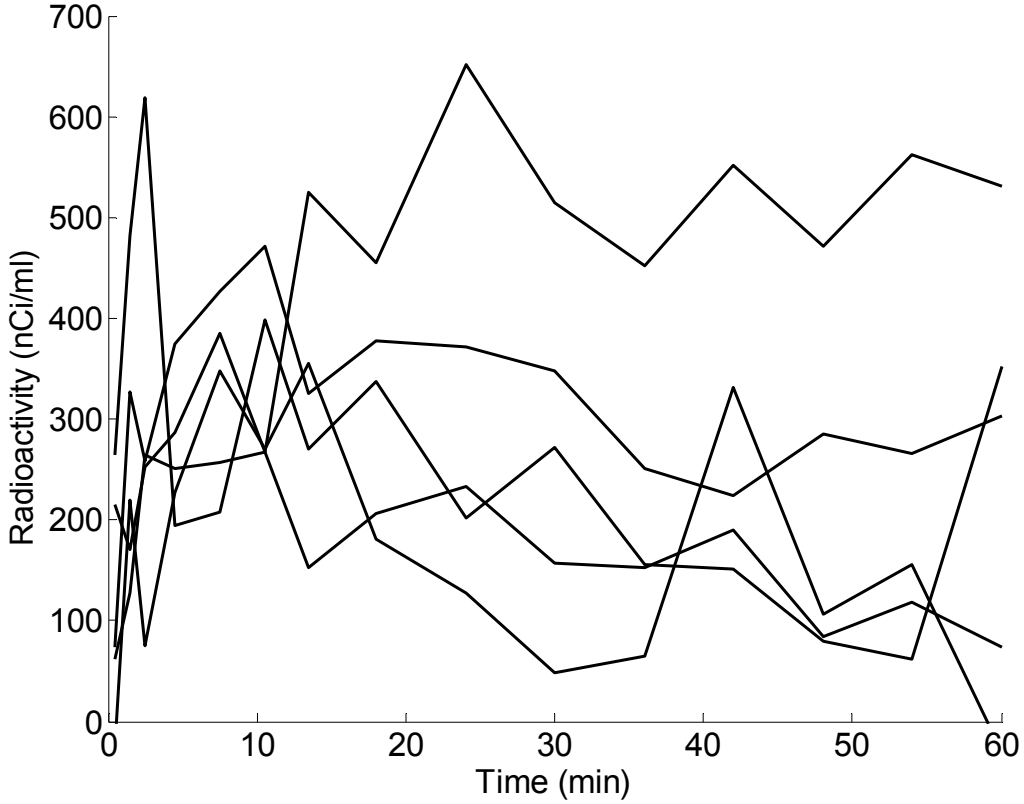

Figure 3

To deal with this problem, first level neuroreceptor studies have to be based on de-noised TAC's to be able to use an arbitrary parameter estimation approach. Alternatively, they need to use special noise-tolerant parameter estimation approaches.

The traditional approach is to define two-dimensional or three-dimensional regions of interests (ROI's) and calculate the mean radioactivity within that region for all timeframes of the PET measurement. This results in regional TAC's, which are virtually noise free such as those in Figure 2. Hence these curves can be analysed using various parameter estimation methods including a full two or three tissue compartmental model fit if a plasma input function is available. The advantage of ROI-based approaches is that they are very effective in reducing or clearing noise. Moreover, only a limited number of parameter estimations have to be performed for a PET measurement. The disadvantage is that it is not possible to obtain detailed information on the subregional distribution of the various parameters (no image) and ROI's placed over areas with heterogeneous tissue composition and parameter distribution may be designated with erroneous parameters (user introduced bias).

A more recent group of approaches produces parameter estimates for all voxels of the PET image. Accordingly, they are referred to as *parametric mapping* approaches. One type of receptor parametric mapping approaches couples the noise handling to the actual parameter estimation. An example of this type is Gunn's basis function method (BFM) which is a based on and coupled to the previously developed simplified reference tissue model (SRTM) (Gunn et al., 1997). Another approach of this kind uses wavelet filtering which is tightly coupled to certain linear parameter calculations (Turkheimer, Banati et al.,

2000). The advantage of this type of parametric mapping is obviously that detailed three-dimensional maps of parameter distribution can be generated. However, the computational demands are much higher than in case of the ROI-based calculations and the choice of parameter estimation method is limited.

A second type of receptor parametric mapping approaches seeks to combine the advantages of the ROI-based approaches and the first type of parametric mapping approaches (Ashburner et al., 1996; Kimura et al., 1999; Kimura et al., 2002; Wong et al., 2002; Zhou et al., 2002; Guo et al., 2003; Kimura, 2004; Liptrot et al., 2004). Firstly, it uses the denoising scheme employed in regional calculations in that it takes the mean or average radioactivity of a number of voxels. However, instead of calculating the mean TAC of regionally adjacent voxels it calculates of the mean for voxels with a similar shape of the TAC. This is based on a classification or clustering of voxels. Secondly, like in case of the ROI-based approaches, the choice of parameter estimation method is decoupled from the noise handling since the mean TAC's of voxels in the same cluster are roughly noise free. Thirdly, it produces parametric maps since parameters obtained for each cluster can be back-projected to the locations of voxels belonging to the given cluster.

A drawback of this second type of parametric mapping approaches is that they reduce the resolution in parameter value. Most approaches presented in the literature require *a priori* definition of the number of clusters and can produce a maximum of 10-20 clusters. Consequently, the set of values in the output parametric maps will be limited to that number. A more productive way of classification can be achieved through the use of *unsupervised cluster analysis* (UCA). UCA is an exploratory data analysis tool, which classifies the input data based on similarity between samples (Everitt et al., 2001; Romesburg, 2004). In contrast to supervised cluster analysis, the number of clusters does not have to be defined *a priori*. Larger number of clusters can be generated, thereby increasing the resolution in parameter value. UCA type of classification has been previously used for kinetic parameter mapping, although only for fluoro-desoxyglucose (FDG) studies and with the assumption that clusters have Gaussian-like distribution and that they are evenly dispersed (Kimura et al., 2002).

1.2 SECOND LEVEL OF NEURORECEPTOR STUDIES

The second level processes information produced in the previous level, which are mostly receptor parametric maps. Methods in this level perform a meta-analysis of maps from several individuals, several receptor maps and/or several experimental conditions. The goal of the processing is to create representations highlighting patterns in the multi-dimensional input data. Accordingly, the outputs of this level are referred to as multi-individual, multi-receptor or multi-condition maps. Established previous work relevant to this level performed statistical parametric mapping of differences in ligand binding between groups of individuals with different experimental conditions, such as patients and controls (for some psychiatry-related examples see: Verhoeff et al., 2000; Frank et al., 2002; Moresco et al., 2002; von Spiczak et al., 2005). However, with the increasing radioligand repertoire an increasing number of investigations acquire PET images in the same individual using two or more ligands of different neuroreceptors. This hints the possibility of exploring patterns and relationships between several neuroreceptor systems beyond assessing group

differences. Such data mining tools were in the focus of developments in the present thesis.

The challenge of multi-receptor mapping is the huge amounts of data to be processed. Therefore the goal of elucidating patterns and tendencies can effectively achieved only if the dataset is compressed in a way that the patterns remain recognisable. A similar requirement of data compression arises in many disciplines such as biology, physics, geography, literature, linguistics, sociology, or even economy, informatics, and internet-technology. A well-known solution is to use UCA as in case of receptor parametric mapping. A powerful way of implementing UCA, when huge datasets of high dimensionality are to be analysed, is through artificial neural networks (ANN's) (Everitt et al., 2001). ANN based UCA can, in principle, be applied for methodologies in both first and second level neuroreceptor studies.

UCA is suitable to form the backbone of multi-receptor mapping so that through further processing of compressed data it is possible to generate output multi-receptor representations.

2 AIMS

The major objective of the thesis project was to enhance our repertoire of computational tools to perform first and second level neuroreceptor studies.

More specifically, the aims were to:

- develop binding parameter, primarily BP, mapping approaches for *in vivo* PET neuroreceptor examinations.
- evaluate such approaches to assess the validity and reliability of estimated BP values in relation to results obtained with the traditional ROI-based approach.
- assess whether these BP mapping approaches qualify for heavy-duty use in applied studies.
- develop UCA methodology using an ANN model that is suitable for performing cluster analysis on huge datasets with possibly high dimensionality within the context of first or second level neuroreceptor studies.
- develop frameworks applying this ANN based clustering methodology for the purpose of binding parameter mapping and, separately, multi-receptor mapping.

3 THEORY AND METHODS

3.1 OVERVIEW OF DEVELOPED METHODOLOGIES

3.1.1 Wavelet-based receptor parametric mapping

3.1.1.1 Overview of wavelet theory

The wavelet analysis of signals resembles the better-known Fourier analysis. According to the Fourier theorem any signal can be made up by the superposition of a set of sinusoids with properly chosen amplitudes and phases (see e.g. Bracewell, 2004). To put it in a different way, the Fourier transform allows for the description of a given signal in the frequency domain by extracting the different frequency components of the signal. However, it is not able to detect the location of non-stationary or transient components within the sample. Because of this a Fourier transform of an image, which contains a great number of transient components such as edges or boundaries, is not easily suitable for localisation of spatial features.

Wavelets, in essence, resemble sinusoids but restricted to a compact, bell-shaped envelope (Figure 4). This restricted nature of wavelets enables them, by contrast to Fourier sinusoids, to detect both the frequency and the location of patterns in the signal. Therefore a coefficient of a wavelet transform is a quantity describing the signal at a certain location with a certain scale (called "spatial frequency") (Mallat, 1989; Daubechies, 1992; Meyer, 1992; Turkheimer et al., 1999).

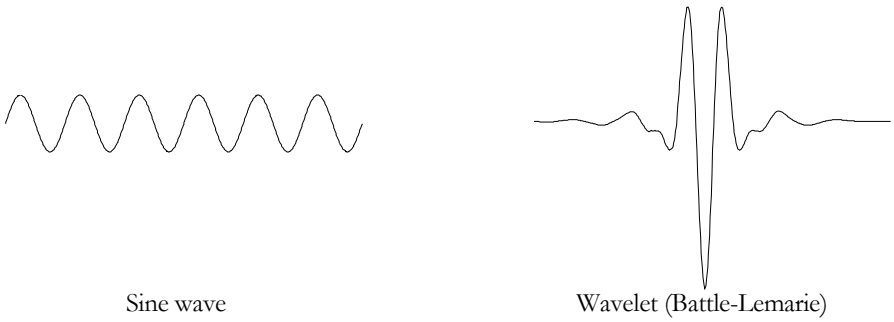

Figure 4

Importantly because of this property, the wavelet transform is capable of separating signal components (lower frequency) from noise (higher frequency) as the components show up in different coefficients of the transform. Another property of the wavelet transform is that it "accumulates" the signal in a few large coefficients whereas the noise is spread in a large number of small coefficients. Therefore small coefficients can be safely disregarded without the loss of the information content of the signal. Taken together, these two properties mean that the "noise" coefficients are not only separate but also they can be identified and deleted because of their low value.

Furthermore, the wavelet transform is a linear operator and thus, if applied spatially on each timeframe of a four-dimensional PET image separately, the original temporal kinetics of the radiotracer is left undisturbed (Turkheimer, Banati et al., 2000). In other words a kinetically homogenous region of the brain, such as a high receptor density structure with a

distinct TAC, will be represented with a wavelet coefficient that exhibits a TAC with the same characteristics. On the other hand noise "patterns" give rise to coefficients that do not show any comprehensible temporal relationships. Noise TAC's can thus be identified when the kinetic analysis is initiated and corresponding coefficients set to zero.

3.1.1.2 Overview of the wavelet transform and wavelet-based parametric mapping

The wavelet transform is realized through an iterative decomposition algorithm known as the dyadic discrete wavelet transform (dyadic DWT) (paper **I**) (see also Mallat, 1989; Unser et al., 1995; Turkheimer et al., 1999). The algorithm for decomposing a one-dimensional signal has the following major steps (Figure 5a):

1. *Convolution.* The data is passed through a lowand and a highpass filter (called wavelet filters) by convolving with the wavelet filter kernels and creating subbands A_1 and D_1.
2. *Downsampling.* A downsampling is then performed on the subbands, since the amount of information is duplicated in the first step.
3. *Iterative repetition.* The first and second steps are repeated, always using the downscaled output of the lowpass filter (A_n) as input for the next iteration or next level. The new outputs (A_{n+1} and D_{n+1}) always replace the input from the previous level. The number of iterations is referred to as the depth of the decomposition.

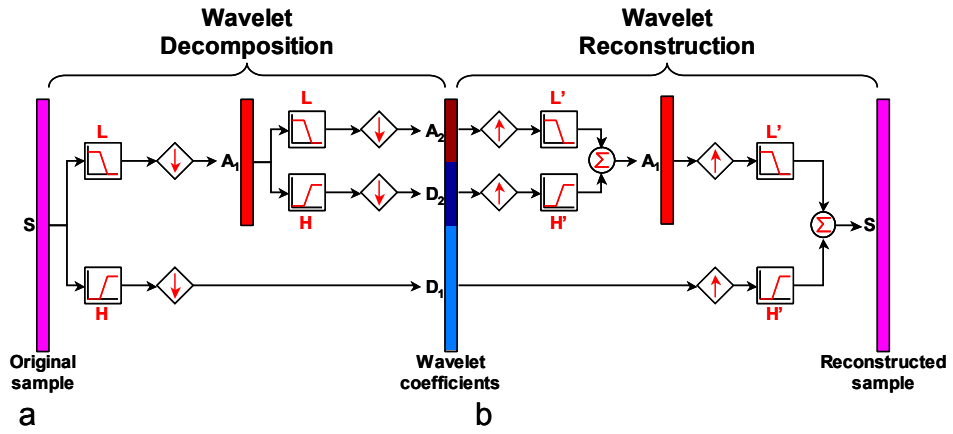

Figure 5

The reconstruction procedure is basically the inverted version of decomposition (Figure 5b):

1. *Upsampling.* The coefficients of the deepest level are upsampled. This compensates for the downsampling step of the decomposition.
2. *Convolution.* The upsampled subbands are convolved with reconstruction low- and highpass filters, respectively. These reconstruction filters are close relatives of the decomposition filters.
3. *Summation.* The output of the two filters (A_n and D_n) is summed to yield the input for the reconstruction lowpass filter on the next level (A_{n-1}). As we mentioned this subband was deleted during decomposition.

4. *Iterative repetition.* The procedure is repeated using the freshly reconstructed A subband and the corresponding stored D subband of the next level. At the coarsest level we end up with the reconstructed sample, which is an approximation of the original sample.

The procedure can be applied to two- and higher dimensional (spatial) samples resulting in two- or higher-dimensional wavelet decompositions. If employed in two dimensions, i.e. on an image, the low- and highpass filters have to be applied sequentially. They are first applied on the rows of the image, resulting in two row-filtered images. Then they are applied on the columns of both row-filtered images, leading to four two-dimensionally filtered subbands or quadrants. One quadrant comes from the application of the lowpass filter on both the rows and the columns. Two quadrants come from the application of both the low- and the highpass filters but in different order. The final quadrant is the output of the application of the highpass filter on both the rows and the columns. The input of the next level is again the quadrant that was lowpass filtered along each dimension.

The method can be extended to three-dimensional samples, such as a three-dimensional timeframe of a PET image. In this case the output at each level contains eight subbands or "cubes" of coefficients corresponding to the number of permutations by which the low- and highpass filters are applied to the three dimensions separately (Figure 6).

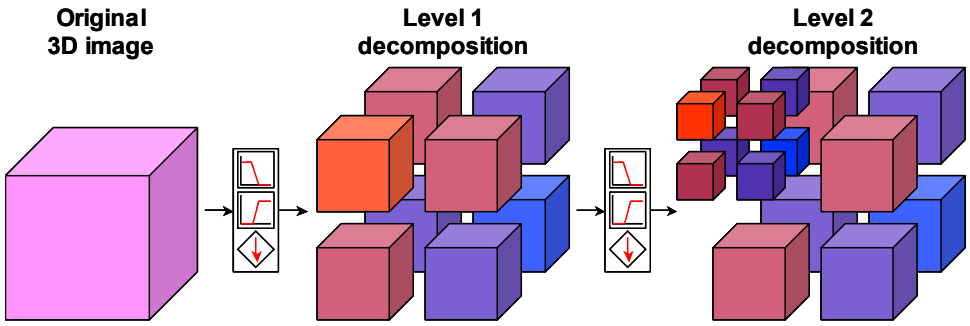

Figure 6

The essential component of the procedure is the specific wavelet filter used for the transform. There are many families of wavelets, each having its own characteristics such as different filter lengths corresponding to different spatial (and frequency) detection properties. According to previous works, the wavelets best suited for analysis of emission tomographic images belong to the family of orthogonal spline wavelets, more precisely the so-called Battle–Lemarie wavelets (Figure 4b) (Battle, 1987; Lemarie, 1988; Turkheimer et al., 1999).

A drawback of the traditional dyadic wavelet algorithm is that low-quality or noisy inputs can be distorted by the downsampling step resulting in artefacts. The presence of the artefact will be the result of a particular "constellation" of the underlying signal and the data-points that were deleted during downsampling. As a consequence if the input is shifted by one data-point and the decomposition is performed again then the artefacts may disappear in certain locations of the sample (but others could at the same time appear in different locations). There is a special version of the dyadic wavelet transform, which is free from this limitation. This is often referred to as the property of *translation-invariance*. In

case of the three-dimensional transform, however, the translation-invariant approach is not workable at present due to the highly increased computational and storage requirements. On the other hand it has been shown that the three-dimensional wavelet transform, by utilising information in all the three principal axes, highly compensates for the lack of translation-invariance with regard to the quality of the decomposition (Turkheimer, Brett et al., 2000).

The estimation procedure used in the thesis is a modification of that described in the literature by Turkheimer (Turkheimer, Banati et al., 2000). The flowchart of the parameter estimation procedure is shown in Figure 7.

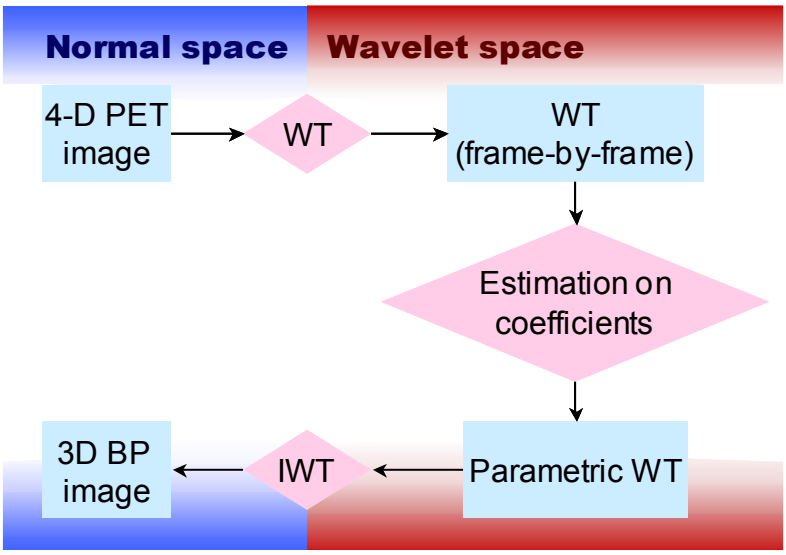

Figure 7

The original images are transformed frame-by-frame to wavelet space using a wavelet transform (WT). The coefficients TAC's of the resulting "dynamic" wavelet transform are analysed quantitatively using a linear binding parameter estimation approach. The end product is a parametric wavelet transform describing the distribution of binding parameters (for example DVR or BP). In the final step wavelet reconstruction is applied on the parametric transform to yield the 3D parametric map of binding parameter values in normal space.

The parameter estimation must be combined with a thresholding of noise coefficients. One possibility is to use information on the statistical uncertainty of estimated parameters to identify "noise" coefficients (Turkheimer, Banati et al., 2000). An alternative way is to pre-categorise coefficient TAC's as either valid (signal) or invalid (noise) (papers **I** and **II**) and then perform parameter estimation only on the valid coefficient TAC's.

3.1.2 Artificial neural network based methodologies

3.1.2.1 Overview of the growing adaptive neural gas model

A popular choice of implementing UCA is through a network model called self-organizing map (SOM). However, SOM's assume a folded two-dimensional topology in the data and are unable to map the local density distribution of the data and thus to detect clusters appearing at widely different density scales. These properties are desirable when using

UCA for neuroreceptor studies. Therefore a novel ANN model was developed called growing adaptive neural gas (GANG) (paper **III**).

GANG is a hybrid model, which employs two, previously proposed SOM-related techniques. The two base models are the *growing neural gas* (GNG) (Fritzke, 1994, 1995) and the *adaptive resolution clustering* (Firenze and Morasso, 1994; Firenze et al., 1994; Schenone et al., 1996) models. The GNG model is an incremental SOM, i.e. the network initially contains only a minimal number of units (usually 2) and the network undergoes a growing in parallel to the training of the units. The units of the network are connected by edges, which are introduced to map and represent the topology of the input data via a competitive Hebbian learning (Martinetz, 1993; Fritzke, 1995).

The GNG network can map the dimensionality and topology of the input data and is able to grow to accommodate larger datasets. However, it does not have a built-in local or global termination criterion. A "global performance criterion" or a target network size must be specified to conclude the growing. This, together with the fact that it does not take into account the variable scales of target clusters of the input data, can lead to "overgrowing" in dense areas and "starvation" in sparse areas of the input space.

The adaptive resolution clustering technique was described as an extension of existing SOM models with adaptively modified *receptive fields* (RF) (Firenze and Morasso, 1994; Firenze et al., 1994). The adaptive RF is able to map the radial dispersion of the data around the units of the network and its effect is that the network adapts to different scales or resolutions of different regions of the input data. However, the SOM model used in the proposal for the adaptive RF was a network with fixed number of units and no topology representation (edges) and therefore it lacked the capability of mapping input dimensionality and topology. GANG implements the feature of adaptive RF's in the model of growing neural gas and hence joins the advantages and overcomes the disadvantages of these two techniques.

A GANG network consists of a set of network units. The network is comprised of:

- weight vectors or the positions of the units in the input space,
- receptive fields of the units that are described by two parameters α and r. The r parameter corresponds to the radius of the RF and the α parameter defines the "steepness" or gradient of the boundary of the RF. The α parameter can have a value in the range 0 to r and high values yield a sharp boundary, low values result in a RF that is less localised. The ratio $ce=\alpha/r$ is the *capture effect* of the unit, and units with a high ce and low r value have a well-localised RF, they are said to be captured by the input. Figure 8 illustrates the concept of RF and the capture effect. The curve displays the boundary of the RF, i.e. the sensitivity of a unit to signals acting on it from different distances; signals close to the unit can activate the unit completely, more distant signals can reach less activation, and those outside its RF fail to activate it at all. The capture effect is demonstrated by plotting the boundary curve for both high and low values of r with corresponding low and high values of ce,
- connections between pairs of units (edges).

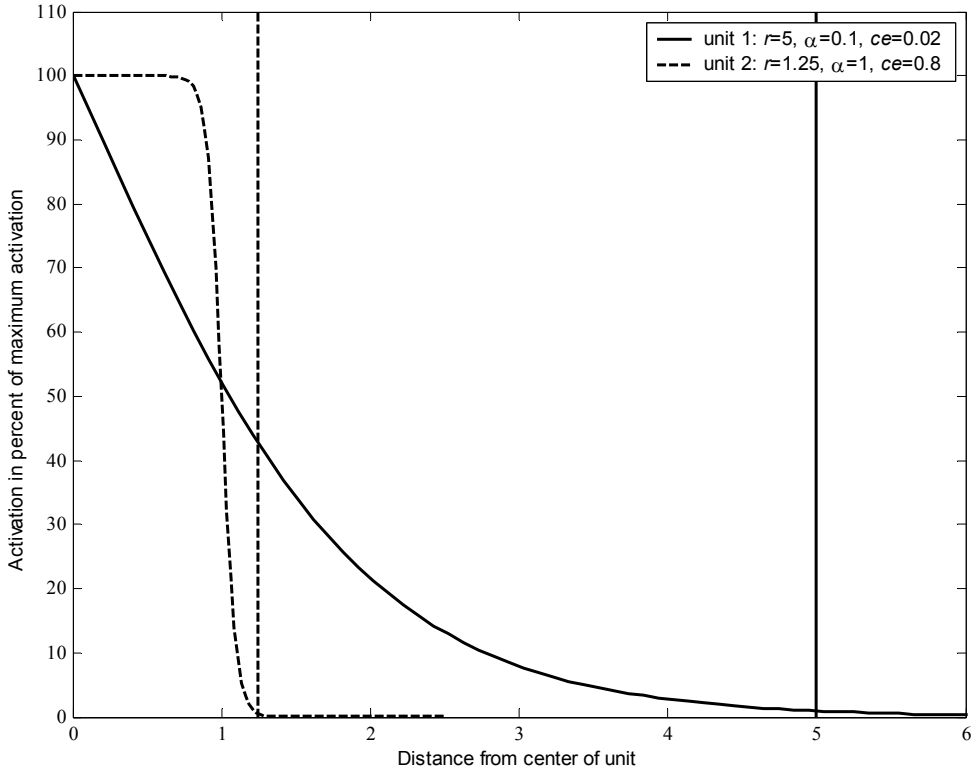

Figure 8

GANG networks are created via the process of growing and fine-tuning. The input for these training phases is a finite or infinite set of *n*-dimensional points that has an unknown probability distribution.

The goal of the GANG training process is defined as an error limit that has to be reached by possibly all units of the network (E_{goal}). This is the "force", which is directly guiding unit insertion or network growth (see the description of the algorithm below, especially steps V/e and VI/a).

The idea of the growing phase is to start with a minimal-sized network and then increase the size of the network through the process of adjusting the positions and RF's of the units and calculating local statistical measures that enable the algorithm to introduce new units at appropriate locations of the network. Furthermore, the edges between the units are created, "aged" or deleted suitably, the latter possibly also leading to the deletion of some network units.

The fine-tuning phase is analogous to the growing phase in that the positions and RF's of the units are still updated. However, the magnitude of the changes made to these parameters is smaller and no new units are introduced to the network.

Figure 9 presents the schematic outline of the growing phase of the GANG model. The following is a description of the model where major blocks of the description (listed using roman numbers) correspond to boxes in the flowchart:

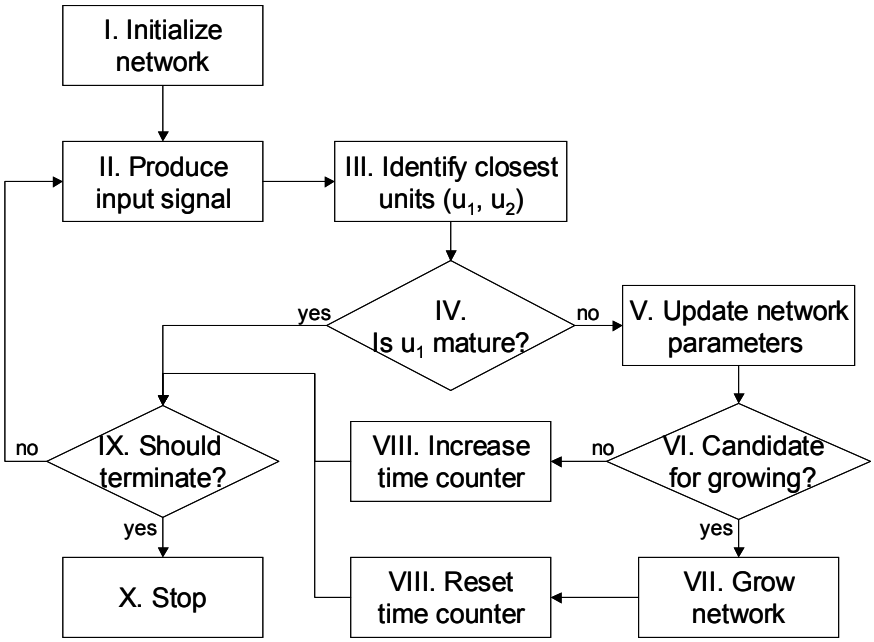

Figure 9

I. Initialize network:
   a. Begin with two network units with random positions and a single edge between them. Set the *r* parameter of the RF to the diameter of the dataset. Set the α parameter to 1% of the diameter of the dataset.

II. Produce input signal:
   a. Produce an input point according to the probability distribution of the data. This distribution is approximated by randomly picking one of the input points.

III. Identify closest units:
   a. Find the closest (u_1) and second closest (u_2) units to the input point (measured as Euclidian distance).
   b. Set the age of the edge between u_1 and u_2 to zero (create an edge if there is none).

IV. Maturity check:
   a. All units have a flag indicating if they are "mature", i.e. they have reached the error goal. Check if u_1 is mature. If u_1 is mature then continue processing normally to step IX/a but the delete the input point from the dataset. Hence this input will be ignored subsequently.

V. Update network parameters:
   a. Add the squared Euclidian distance between u_1 and the input point to a local error measure.
   b. Increase a hit counter for unit u_1 by one (see next step).
   c. Update variables of the unit that can be used later to estimate the *average location of closest points* for each unit using the hit count.
   d. Update the RF of u_1 and u_2. The updating scheme ensures that the *r* radius of the RF is set in accordance to the distances of all the points closest to the given unit and the α parameter gets close to the *r* parameter if the closest

points are mainly inside the radius and vice versa (thus capturing or "un-capturing" the unit).

e. Update the maturity flag by setting it for all units whose average local error is less than the goal error limit E_{goal}.

f. Find the topological neighbours of u_1 (units connected by an edge to u_1).

g. Update the weights (positions) of u_1 and u_2 (or alternatively u_1 and all its topological neighbours). The updating scheme moves the closest and the second closest units (or the topological neighbours of u_1) toward the input point with a fraction of the distance to that point. The scheme also utilises the RF of units by calculating an "activation" parameter. This parameter ensures that units become "insensitive" to points lying outside the radius of their RF. This effect was demonstrated previously in Figure 8.

h. Increment the age of all edges originating from u_1 (except for that going to u_2).

i. Increment the age of all edges that connect units that were never or very few times identified as the "closest unit" (hit counter is zero or low). This ensures that units, which were created or end up in empty regions of the input space and thus do not receive inputs, will eventually "die out".

j. Delete all edges that are older than the certain maximum "age". If this step yields units without emanating edges then delete those units also.

VI. Check for a candidate for growing:

a. Find the unit with the largest average local error measure. If there are no such units then go to step VIII/a

b. Find the topological neighbours of this unit.

c. If this unit is mature or very young or all of its neighbours are very young then skip growing and go directly to step VIII/a.

VII. Grow network:

a. Estimate the average location of all points closest to the unit found in step VI/a.

b. Find the topological neighbour of this unit that lies in the direction of the average point (maximum 90 degrees off direction).

c. Insert a new unit. The new unit is inserted halfway between the two units and it is connected with an edge to both of them. The original connection between the two existing units is deleted. Initialise other parameters of the new unit appropriately.

VIII. Update time counter:

a. If a new unit was inserted in this iteration and it resulted in a *net* increase in the number of units (more units than any time before) then a "time" counter is set to zero. Otherwise this counter is increased by one. This measures the "time" since the last net growth of the network and it is more informative than simply the "time since last unit insertion" because units could have been deleted and added *without* reaching a greater size.

IX. Termination check:

a. Check if the growing epoch should be terminated. Possible reasons for termination:

- No more input signals.

- All units are mature, further growing is not possible.
- Not enough input points left for good quantization. For this, estimate the number of input points per unit in the growing part of the network by dividing the number of units that are immature with the number of input points left.
- No *net* increase in the number of units for a predefined number of adaptation steps, i.e. the "time" counter is greater than a predefined limit. This limit can be set to the total number of input points to be on the safe side. This termination criterion helps to avoid possibly infinite iterations with no convergence toward reaching the goal. In other words, the growing of the network may be terminated before it could reach the goal set by the target error limit (E_{goal}).

b. If any of these conditions is met then go to step X/a. Otherwise continue the growing epoch, i.e. go to step II/a.

X. Stop:

a. Optionally prune units with a low *ce* from the network. These are very young, non-captured units, which can be assumed to have a bad quantization profile.

b. Finish.

By the end of the growing process the network is roughly ready; the units have mapped the distribution and the topology of the input data. There will be many units with small RF's in the dense regions of the input space and a few units with large RF's in the sparse regions of the input space.

In the second, optional training phase no new units are created but the processes of edge handling, RF modulation and position adjustment are still working. This leads to the fine-tuning of the GANG network. The individual units and their RF's of the final GANG network are referred to as *neighbourhoods*.

E_{goal} is the main parameter influencing overall network growth and thus the final number (and distribution) of network units. The value of E_{goal} must be set in accordance with the intentions of the application and the characteristics of the dataset. Large values result in a smaller GANG with possibly no units in sparse areas since neighbouring units in denser areas "cover" input points from sparse areas while their local error is still under E_{goal}. Very small values can result in huge GANG's although sparse areas are guaranteed to have their own units. A way of finding the "best" E_{goal} for each dataset is to make several training sessions using smaller and smaller values until all regions, including sparse ones, are sufficiently mapped.

3.1.2.2 GANG based receptor parametric mapping

This approach is a novel variant of cluster analysis based parametric mapping where the classification of voxel TAC's or derived variables is implemented using the GANG model (paper **IV**). Similarly to other methods in this field, parameter estimation is performed on average TAC's of clusters and the estimated parameters are back-projected to the spatial locations of the voxels using the classification.

Figure 10 displays the flowchart of the approach. The approach comprises the following steps:

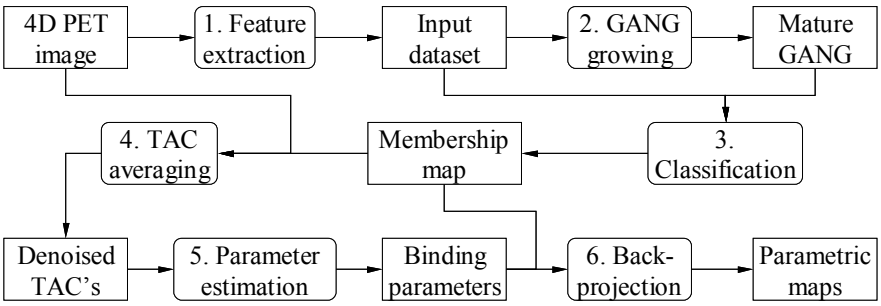

Figure 10

1. Feature extraction:
   The essence of the proposed approach is the classification of voxels according to the similarity of their kinetic behaviour. Therefore the variables for subsequent processing must reflect the kinetic properties of voxels, i.e. they represent features of the PET image that are important for the analysis. Hence the name *feature extraction*. The most obvious set of such feature variables are the frame-by-frame radioactivity values of voxel TAC's. Other such variables can be the area under the curve (AUC) of a given voxel's TAC or the voxel values in the summation image, which are still easy to obtain. These two quantities are similar but the summation image is usually an integral of only some last part of the whole duration of the image acquisition thereby focusing more on the period of binding equilibrium.

   The number of variables selected for feature extraction defines the dimensionality of the input space for further processing. For example, in case of selecting the voxel TAC's of a 15-frame PET image the input space will be 15-dimensional. To drive the sensitivity of the classification towards some of the variables they can be scaled or weighted. For example, weighting can be beneficial when raw voxel TAC's are used as feature variables (Guo et al., 2003). The other way around, the variables can be normalised to have a more balanced effect on the classification.

2. GANG training and growing:
   The distribution of data in the extracted feature space is mapped using GANG network grown on the dataset. As described in section 3.1.2.1, the GANG network model is capable of classifying the input into a large number of neighbourhoods in arbitrary dimensional data-space. The neighbourhoods are usually smaller than what is defined as a well-delineated cluster of the input in traditional cluster analysis.

   An important property of mapping data distribution using the GANG model is that it can detect the presence of sparse regions in the input data. This feature can be advantageous if sparse areas represent a distinct, important subset of the input. Such distribution can be expected in case of the input datasets used for binding parameter mapping. The reason for this is that some neuroreceptors can have very high concentrations in relatively small anatomical regions in the human brain, for example the striatum for dopamine D_2 receptors. Thus the feature extraction performed on a PET image of such a receptor will have only a limited number of points in the corresponding areas of feature space.

3. Classification:
   After the growing and training phase, the input data is classified using the GANG network. This means that each input point is assigned to the closest GANG unit or neighbourhood. This classification thus defines a one-to-one correspondence between neighbourhoods and subsets of input points. Furthermore, individual input points also have a one-to-one correspondence to specific voxels in the space of the PET image. Therefore the classification also defines a mapping from neighbourhoods to subsets of voxels and *vice versa*. This mapping is referred to as a *membership map*.

4. TAC averaging:
   The membership map allows the selection of subsets of voxel TAC's with similar kinetic behaviour. Thus averaging TAC's of the same subset results in TAC's with diminished noise.

5. Parameter estimation:
   The parameter estimation is performed on noise-attenuated TAC's. Therefore any method of estimating binding parameters may be applicable that one can use in the classic ROI-based approach. Parameters from either reference region or blood input kinetic models may be estimated.

6. Back-projection of parameters:
   The resulting binding parameters are back-projected to the space of the PET image using the membership map from the classification (step 3). Thus the approach finally yields three-dimensional maps of binding parameters.

3.1.2.3 GANG based multi-receptor mapping

The proposed approach of multi-receptor analysis is a data exploration tool based on unsupervised cluster analysis using artificial neuronal networks (paper **V**). The input to the analysis consists of 3-dimensional BP maps of different receptor systems for each subject included. Similarly to GANG based parametric mapping, the voxels of the anatomically standardized brain images can be projected to a feature space where each axis corresponds to a certain feature of a voxel in the input datasets. The simplest of such feature variables is the BP value. More complicated feature variables can be constructed from various feature-measures such as BP ratio or local BP voxel statistics such as variance, gradient magnitude, etc. When the feature space has been defined, each individual's anatomically standardized BP maps can be projected to that space. The task is then to extract information from this multi-dimensional data set with a main focus on patterns of inter-individual changes of the projected location of voxels. Grouping of voxels in feature space is desirable not only due to the huge amount of data but also in order to facilitate the emergence of more stable and consistent patterns. Furthermore, it brings about the possibility of quantifying the distribution, spread and density of data points in different areas of feature space.

As described in the introduction section, the exploration of multi-receptor feature spaces should ideally be performed using a data mining tool that is (i) unsupervised, (ii) unbiased, (iii) requires no *a priori* hypothesis, and, at the same time, is (iv) data-driven, reduces the burden of data into manageable "piles" and identifies intra-data associations, patterns or tendencies. A well-known tool, which meets many of these requirements, is

UCA. The purpose of UCA is to classify input data based on similarity between samples. This is what can be referred to as *transverse processing*.

A GANG based UCA is utilised in the proposed approach with the following considerations. The cluster structure of multi-receptor data is rather arbitrary due to the continuous spread of receptor density values over a certain range. Accordingly, the technique works on a presumably "sub-cluster" level with the entities of UCA corresponding to neighbourhoods of the GANG network. This lends the name *neighbourhood analysis* to the initial part of the approach.

After the classification of multi-receptor patterns, the approach analyses the tendencies of inter-individual changes of these patterns. This *longitudinal processing* requires an extension of basic UCA methodology. The inter-individual changes of multi-receptor patterns are called *trajectories*. *Trajectory analysis* offers a composite look on the multi-individual, multi-receptor data set at hand.

The following is a detailed description of the process of the proposed approach for multi-receptor analysis (see flowchart in Figure 11).

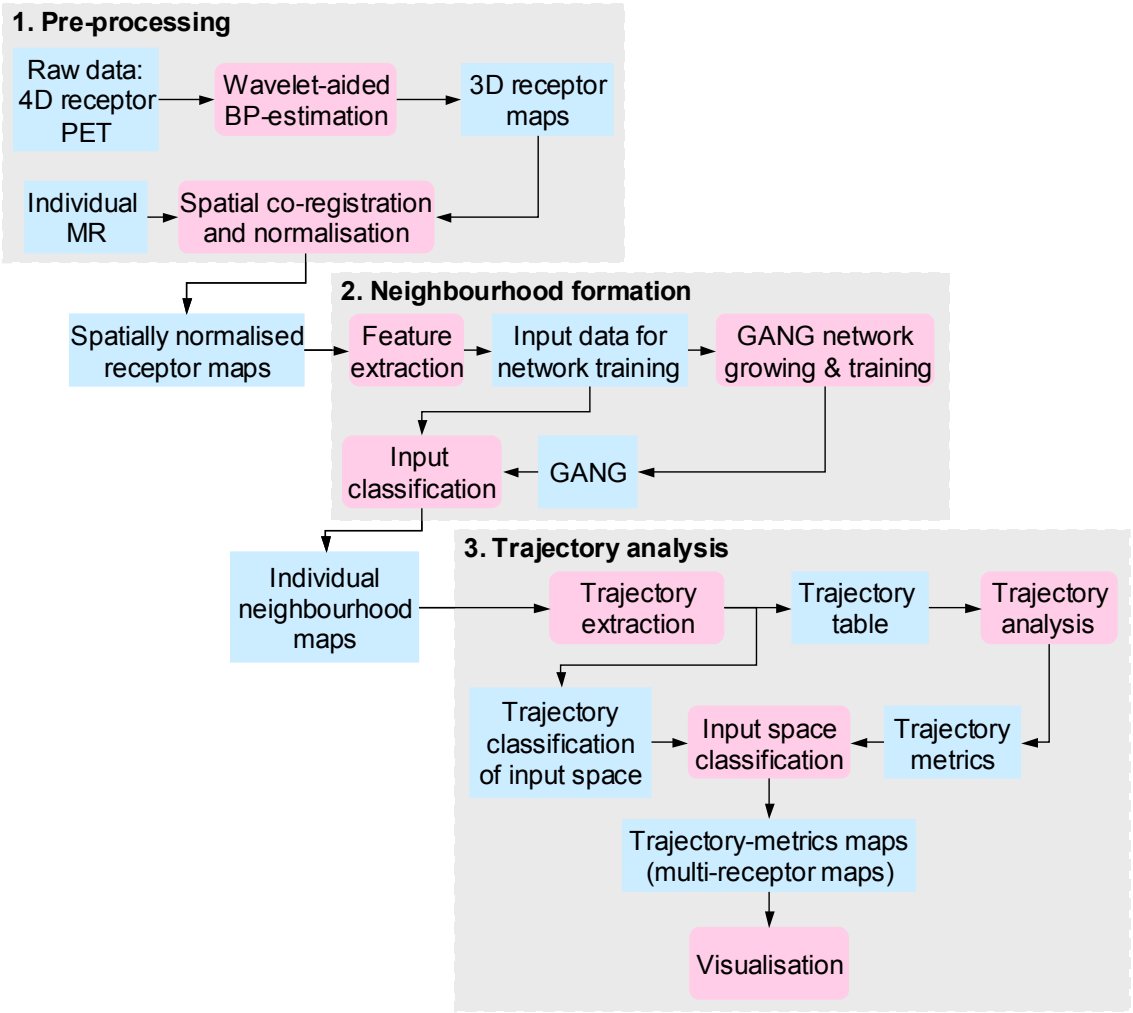

Figure 11

1. Pre-processing:
   Three-dimensional receptor BP maps are created from the raw 4D receptor PET images using a wavelet-aided BP-estimation framework presented previously (paper **I**, Turkheimer al. 2000). The individual BP maps are spatially co-registered and normalized using the individual MR images of the subjects.

2. Neighbourhood formation:
   The local image intensity (BP value) is extracted from the spatially normalised BP maps. Only those voxels are included for which there is at least one individual where the BP value for both receptor types is greater than zero. These feature variables constitute the input for the neighbourhood analysis, which is performed by the GANG network (paper **III**). The trained network subdivides the input space into neighbourhoods. Thus each input point in feature space can be assigned to one of the neighbourhoods. Each input point in feature space has a corresponding voxel in normalised image space. Thereby classifying the input data in feature space results in the creation of individual *neighbourhood maps* in image space.

3. Trajectory analysis:
   Each voxel in standard image space has a corresponding neighbourhood in feature space in each individual. The collection of the centres of these neighbourhoods in feature space defines a *trajectory*. The trajectories are enumerated and sorted. The enumeration defines a classification (*trajectory classification*). In the next step different metrics or properties of the trajectories are calculated such as:

   - *Exclusivity index*: since each neighbourhood is comprised of feature vectors from one or more individuals, it is possible to determine the subject who has the most contribution to any given neighbourhood. This is the "*owner*" of the neighbourhood. Knowing the "owner" it is also possible to calculate an index, which represents how many times more contribution the "owner" has to the given neighbourhood than all the others. This defines the exclusivity index. It is a measure of the "*individuality*" of the brain with regard to the others in the study. The more neighbourhoods are "owned" by a given subject the more distinct multi-receptor patterns he or she has compared to the others.
   - *Average Euclidian distance*: it is calculated as the mean of the (Euclidian) distances between the centres of any two of the neighbourhoods in a given trajectory. This metric has to do with the expected "*stability*" of multi-receptor patterns. Larger values indicate greater inter-individual variations and vice versa.
   - *Mean voxel count*: it is the mean number of voxels in the neighbourhoods of a trajectory. This metric shows which brain regions contain voxels corresponding to desolate or densely populated neighbourhoods of the feature space.
   - *Mean neighbourhood density*: it is calculated via dividing the voxel counts with the area or volume of the neighbourhoods in a given

trajectory. There can be the large variations in neighbourhood density.

- A*verage topological distance*: this metric gives the average number of neighbourhood boundaries that have to be crossed to get from any one neighbourhood of a trajectory to another.
- *Total number of neighbourhoods*: it is the number of neighbourhoods in a trajectory. Trajectories with a lower value may indicate more stable multi-receptor patterns and *vice versa*.
- *Total volume of neighbourhoods*: it is the sum of the volumes of the neighbourhoods that make up a trajectory.
- *Correlation coefficients of trajectory*: if the feature variables used to set up the analysis are simply the BP values then the neighbourhoods of the feature space offer a quantized representation of the dataset. Therefore they are also useful for the calculation and visualisation of properties that are normally calculated on the voxels themselves. An example for this is the analysis of correlation between feature variables of the neighbourhood centres in a trajectory.

Using the trajectory classification these various trajectory metrics can be back-projected into normalised image space resulting in "trajectory-metrics" maps. These maps comprise information on multiple receptor systems and individuals therefore they are referred to as *multi-receptor maps*.

3.2 DATA COLLECTION

3.2.1 Subjects

The PET images used for the thesis work were from studies approved by the Ethics and Radiation Safety Committee of the Karolinska Hospital (papers **I**, **II**, **IV** and **V**). Healthy subjects were enrolled and informed consent was obtained in line with the Declaration of Helsinki. The subjects were healthy according to history, medical examination, blood and urine screening tests and magnetic resonance imaging (MRI) of the brain. None of them were taking medications.

3.2.2 Magnetic resonance imaging

The MR system used was GE Sigma, 1.5 Tesla. Proton density, T_1- and T_2-weighted images were obtained. Subjects had an individual plastic helmet that kept the head in a fixed position during data acquisition (Bergstrom et al., 1981).

3.2.3 Positron emission tomography

The PET system used was a Siemens ECAT Exact HR machine, which provides 47 slices with a center-to-center distance of 3.125 mm. The intrinsic spatial resolution is 3.6 mm in plain at the centre of the field of view and 4.0 mm full width at half maximum (FWHM) axially (Wienhard et al., 1994). The same head fixation system as in the MRI measurement was used in PET to yield the same positioning of the head in both modalities.

The radioligand was injected as a bolus into the right cubital vein. The images were reconstructed using filtered back-projection with a Hanning filter with a cut-off frequency 0.5 of maximum, providing an in-plane resolution of 5.5 mm FWHM. Image matrix size

was 128 × 128 and pixel size was 2.0 mm. Scatter correction was performed as described in the literature (Wienhard et al., 1994). Attenuation correction was performed using a transmission scan obtained for each individual.

3.2.3.1 [^{11}C]FLB 457 images

[^{11}C]FLB 457, a high-affinity radioligand of dopamine D_2/D_3 receptors, was prepared as previously described (Halldin et al., 1995) (papers **I**, **II**, **IV**). The specific radioactivity was 1081-2086 Ci/mmol at time of injection. Total injected radioactivity was 189-299 MBq, which corresponds to an injected mass of 1.1 to 2.1 μg. After injection of [^{11}C]FLB 457 data were acquired for 63 min in consecutive time frames. The frame sequence consisted of three 1-minute frames, four 3-minute frames and finally eight 6-minute frames.

3.2.3.2 [^{11}C]WAY100635 images

[^{11}C]WAY100635, a ligand of the post-synaptic $5HT_{1A}$ receptors, was prepared as previously described (Andree et al., 2000) (papers **II** and **V**). The injected dose was 260±78 MBq. The PET measurements were 69 min long, consisting of 15 time-frames: 3 x 1 min, 3 x 4 min, 9 x 6 min.

3.2.3.3 [^{11}C]MADAM images

[^{11}C]MADAM, a ligand of the pre-synaptic serotonin transporters, was prepared as previously described (Chalon et al., 2003) (paper **V**). The injected dose was 302±11 MBq. The PET measurements were 93 min long, consisting of 15 time-frames: 3 x 1 min, 3 x 4 min, 13 x 6 min.

3.3 STUDY DESIGNS

3.3.1 Cross validation study

A cross validation scheme was used for the evaluation of the wavelet-based parametric mapping approach (papers **I** and **II**). PET images obtained using [11C]FLB 457 and [11C]WAY100635 were included in the analysis.

The choice of [^{11}C]FLB 457 for cross-validation purposes was motivated by the fact that the human brain displays a 100-fold range of D_2 dopamine receptor densities across different brain regions (Kessler et al., 1993). [^{11}C]FLB 457 is capable of producing signals from any area within this wide range (Halldin et al., 1995; Farde et al., 1997; Delforge et al., 1999; Olsson et al., 1999; Suhara et al., 1999). Moreover, brain regions with different receptor densities display a wide range of size and shape that may present a further challenge to parametric mapping approaches.

[^{11}C]WAY100635 was selected for similar reasons as [^{11}C]FLB 457. It also provides signals from a number of brain regions with different size and shape and varying receptor densities. However, the pattern of distribution is distinct from that of [^{11}C]FLB 457. Another reason for selecting this radioligand was that [^{11}C]WAY100635 is currently widely applied in clinical studies on the role of the serotoninerg system in neuropsychiatric diseases such as anxiety, depression, Tourette syndrome and schizophrenia (see e.g. Lam et al., 1996; Drevets et al., 1999; Andree et al., 2000).

Each of the individual datasets was analysed by six approaches; the traditional ROI-based graphical parameter estimation, voxel-wise parametric imaging using Logan's original linear graphical plot (PILogan), the version using Varga's modified version

(PIVarga), three-dimensional wavelet-filtering based neuroreceptor mapping approach, Gunn's basis function method (BFM), and the DEPICT approach. Additionally, in case of [^{11}C]FLB 457 images (in paper **I**), a variant of the wavelet based approach using two dimensional wavelet-filtering was also used. The results of the ROI-based approach served as a reference for the evaluation of the other approaches. The following is a short overview of the applied approaches.

3.3.1.1 ROI-based analysis

Images were transformed into standard anatomical space using the computerized human brain atlas (HBA) (Roland et al., 1994). ROI's from the anatomical database of the HBA were positioned for a series of brain structures of interest in the dopaminergic and sertotoninergic systems. The cerebellar cortex was used as a reference region for free and non-specifically bound [^{11}C]FLB 457 and [^{11}C]WAY100635 in brain (Farde et al., 1998; Olsson et al., 1999).

The binding potential was estimated using the reference region version of Logan's graphical analysis (Logan et al., 1996). Distribution volume ratio (DVR) was determined by fitting a line to the linear part of the plot using traditional linear regression. This corresponded to 36-60 min for [^{11}C]FLB 457 and 45-69 min for [^{11}C]WAY100635. The binding potential (BP) was calculated as DVR minus one (Logan et al., 1996; Farde et al., 1998; Olsson et al., 1999).

3.3.1.2 PILogan and PIVarga

PILogan uses the traditional linear regression model also applied in the ROI-based analysis (Logan et al., 1990), whereas the PIVarga approach minimises the sum of squared *perpendicular* distances to the fitted line, as recently suggested by Varga (Varga and Szabo, 2002). To obtain parametric maps, the calculations are performed voxel-by-voxel.

The anatomical standardisation procedure using HBA was performed on the parametric images. In this way no unnecessary sources of error were introduced before the kinetic calculations. For standardisation the same warping transformations were used for each individual as in case of the ROI-based analysis. Having the images in standard space the same ROI's could be applied to determine the average binding potential of the target anatomical structures for cross-validation purposes.

3.3.1.3 Wavelet based analysis

The analysis was performed as described in the overview on wavelets (section 3.1.1.2). For the wavelet transform either the two-dimensional translation-invariant (2DTI) (only paper **I**) or the three-dimensional (3DWT) wavelet transform was applied. The filters for the transform belong to the Battle-Lemarie wavelets (Battle, 1987; Lemarie, 1988). The depth of the decomposition was 2 and the length of the filter kernels was 22. The parameters were chosen in an iterative approach, which yielded the best recovery of regional BP values as well as the lowest computational load.

The coefficient TAC's of the dynamic wavelet transform were analysed quantitatively using Logan's graphical estimation. Pre-thresholding was used to identify noise coefficient TAC's and thus reduce the number of calculations. A 3D mask image of the reference region (cerebellar cortex) was created first and transformed to wavelet space. The AUC of each coefficient's TAC was calculated. This AUC "transform" was then masked with the previously created WT of the 3D mask to yield the AUC value of those coefficients that

correspond to the reference region in normal space. The average value of this pool of AUC values was used as the thresholding limit.

The end product of the calculations in wavelet space was a parametric wavelet transform describing the distribution of DVR. After wavelet reconstruction the parametric map of DVR in normal space was obtained. The BP map was calculated from the DVR map by subtracting one from the DVR values (Logan et al., 1996).

3.3.1.4 BFM

The BFM approach has been described in detail in the literature (Gunn et al., 1997). It is based on the simplified reference region (or tissue) model (Lammertsma and Hume, 1996). It creates a set of basis functions. For each voxel, the basis function which yields the minimal residual sum of squares is chosen to determine the final parameters and hence the unknowns of the model (includeing *BP*).

3.3.1.5 DEPICT

The DEPICT approach has been proposed and described in detail in the literature (Gunn et al., 2002). The basic assumption is that the compartmental model behaves essentially like a linear filtering system as known from the field of signal processing. Such a system can be fully characterised through its *impulse response function*. Accordingly, DEPICT is a data-driven parameter estimation framework that characterises the behaviour of the radioligand in a biological compartmental system in terms of its impulse response function. It derives the compartmental model description of the data from the data itself yielding for each voxel the estimates of coefficients of the compartmental model as well as the number of compartments best describing the local kinetic behaviour of the data.

3.3.2 Demonstration of characteristics

3.3.2.1 Testing the GANG model

The capabilities of the GANG model were demonstrated using different simulated input data (paper **III**). Three artificial datasets were used.

In the first two cases, the input data was a finite set of points in three-dimensional space. The overall topology of distribution was similar, but the local density distribution was different. In particular, the sample data had three regions in terms of topological relations. One region had three-dimensional local topology enclosed in a box. The other regions of the input had only two- or one-dimensional local topology (plane and line, respectively). Furthermore, the region with one-dimensional local topology was separated to a linear and a circular sub-region. This resulted in four distinct data regions in total.

In the first dataset, any one of these four regions had the same number of data points. This means that the 3D density of points was higher in the lower dimensional regions than in the higher dimensional ones. The input contained 200,000 points.

In the second dataset, the 3D density of the input points was more balanced throughout the different regions. Therefore the number of points was orders of magnitude less in the lower dimensional regions than in the higher dimensional ones. For example, only 0.39‰ of the input points were in the 1D linear region. With having a total number of 200,000 points in the dataset this means that there were only 78 points in this region.

The third example used simulated brain MRI data from the *BrainWeb* Simulated Brain Database (Cocosco et al., 1997; Collins et al., 1998; Kwan et al., 1999). In detail, the input

for training was a multivariate dataset that was created from simulated T1-, T2-weighted and proton density (PD) images of an anatomical human brain model containing mild multiple sclerosis (MS) lesions, which served as the sparse region of interest for testing the network models. The input for network training was defined as 3D vectors with x, y, and z coordinates corresponding to T1, T2, and PD image intensities, respectively. Only voxels (and thus feature vectors) inside the brain or the cerebrospinal fluid (CSF) were included using the anatomical model for voxel selection. Thus the total number of input points in feature space was 1,955,621 of which only 420 points (0.21‰) corresponded to voxels with a fuzzy membership value of more than 50% in the class of MS lesions according to the anatomical phantom.

The aim of this example was to highlight important principles of performing GANG-based cluster analysis and image segmentation in a biomedical application. Therefore, full-blown, optimised UCA and image segmentation was not performed nor required. Network units were not used directly as cluster centres for image classification and segmentation. Instead, as in other previous works, the trained networks were processed in a subsequent step to extract groups or clusters of network units (Vesanto and Alhoniemi, 2000; Dittenbach et al., 2001; Flexer, 2001; Kiang, 2001; Daszykowski et al., 2002). This classification enabled the assignment of class membership values to input points via finding the closest network unit and hence the corresponding cluster. The grouping of network units was performed using standard hierarchical cluster analysis (see for e.g. Aldenderfer and Blashfield, 1984). The number of clusters constructed was increased step-by-step until the segmentation gave acceptable demarcation of different healthy brain tissue classes (especially white and grey matter). Accordingly, the number of target clusters was finally fixed at 10.

The GNG model was also trained on the same datasets to enable highlighting the advantages of the GANG model through the comparison of results.

3.3.2.2 Testing the GANG based receptor parametric mapping

A PET image from the dataset also used for evaluating the wavelet-based approach (papers **I** and **II**) was analysed with GANG based parametric mapping approach (paper **IV**). The PET image was obtained using the radioligand [^{11}C]FLB 457. The creation of "denoised" voxel TAC's was performed twice; each time as described in the overview section (section 3.1.2.2) but using two different sets of feature variables. The first set of variables consisted of the 15 radioactivity values in the voxel TAC's plus the AUC value of the TAC. This feature extraction thus yielded a 16-dimensional input dataset for GANG training and growing. The feature variables were normalised to have mean 0 and SD 1. The second analysis used another set of features. On feature variable was, again, the AUC value of the voxel's TAC. The other variable was simply the voxel value in the summation image, which was calculated from the last 10 frames (9-63 minutes after injection). Thus the second extracted input dataset for GANG growing was two-dimensional. The feature variables were not normalised in the second case. Only voxels inside the brain were included in the calculations by selecting voxels with an AUC value greater than 90% of the reference region (cerebellum).

The average TAC's, which are practically noise-free, can be analysed using many different parameter estimation procedures to yield kinetic parameters of interest. Accordingly, the following techniques were applied: the reference region variant of

Logan's graphical BP estimation (RLogan), linearised simplified reference tissue model fit (LSRTM), simplified reference tissue model fit (SRTM), Gunn's basis function method (BFM), Gunn's data-driven estimation of parametric images based on compartmental theory (DEPICT) (used in ROI-based mode) and full plasma-input three-compartmental model fit (PITCM) (Sandberg, 1978; Lammertsma and Hume, 1996; Logan et al., 1996; Gunn et al., 1997; Olsson et al., 1999; Gunn et al., 2002). The PITCM approach directly fitted the values of the k_1, k_2, k_4 and BP parameters using a genetic algorithm optimisation (Goldberg, 1989; Mühlenbein et al., 1991; Georges-Schleuter, 1992). Further parameters (k_3 and total distribution volume, DVT) were calculated from the fitted ones. Finally, the resulting binding parameters and, where applicable, additional output parameters were back-projected to the PET image space.

3.3.2.3 Testing the GANG based multi-receptor mapping

The analysis of two systems belonging to the same neurotransmitter can be regarded as the starting point of a more complex analysis into the multitude of receptor systems. Therefore the multi-receptor mapping approach was tested on receptors of one neurotransmitter: the serotoninerg system, using PET radioligand data regarding both the pre- and post-synaptic (5-HT_{1A}) binding sites (paper **V**). In particular, the study included PET measurements obtained using [^{11}C]WAY100635, a ligand of the post-synaptic $5HT_{1A}$ receptors, and [^{11}C]MADAM, a ligand of the pre-synaptic serotonin transporters.

The analysis was performed as described above in the overview section (section 3.1.2.3). The feature space for the analysis was defined simply as a two-dimensional space with presynaptic BP values on the x-axis and postsynaptic BP values on the y-axis.

4 RESULTS

4.1 CROSS VALIDATION STUDY OF WAVELET-BASED PARAMETRIC MAPPING

The different approaches used in the cross validation studies yielded conspicuous differences between the parametric images created from both the [^{11}C]FLB 457 (papers **I** and **II**) and the [^{11}C]WAY100635 (paper **II**) data. The dopamine D_2/D_3 BP maps created with the PILogan and PIVarga approaches were noisy in appearance. They contained "holes" corresponding to missing estimated BP values. The PIVarga approach also contained a number of outlier values, especially in the area of the striatum a region with high receptor density. These BP values were extremely high such as in the range of 70 to 90. Figure 12 displays the estimated regional D_2/D_3 dopamine receptor BP values of the tested parametric mapping approaches in percent of the corresponding value of the reference method and in increasing order of receptor density (n=10; mean + SD). Figure 13 displays horizontal cross-sections through the summation image and dopamine D2/D3 BP maps of the same individual obtained using the compared approaches (papers **I** and **II**).

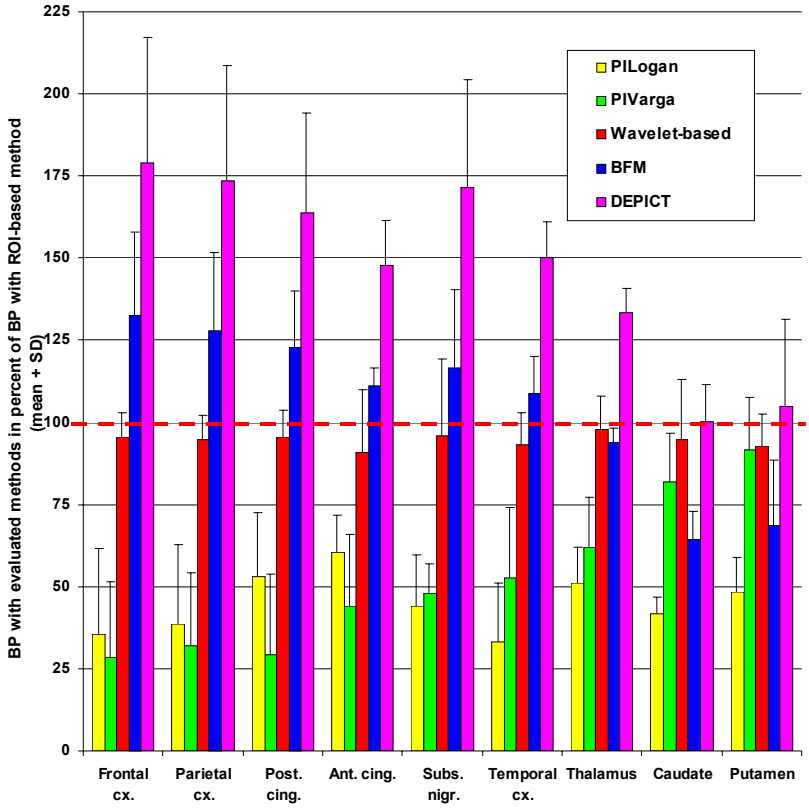

Figure 12

In case of the PILogan approach the average regional BP values were lower than the corresponding ROI-based values for each region (papers **I** and **II**). The PIVarga approach showed a similar pattern with the exception of high-density regions where the BP values were higher than those of PILogan but still lower than the values of the ROI-based approach (paper **II**).

Both the 2DTI (paper **I**) and 3D (papers **I** and **II**) wavelet-based approach yielded noise-free BP maps, although the sharpness of the images was less than that of the summation image. The parametric maps based on the 3DWT-aided analysis showed more homogeneous patterns (especially in the axial direction) than those coming from calculations with the plane-by-plane 2DTI wavelet transform (paper **I**). The estimated regional BP values were about 78% (2DTI) and 95-100% (3D) of those with the ROI-based approach.

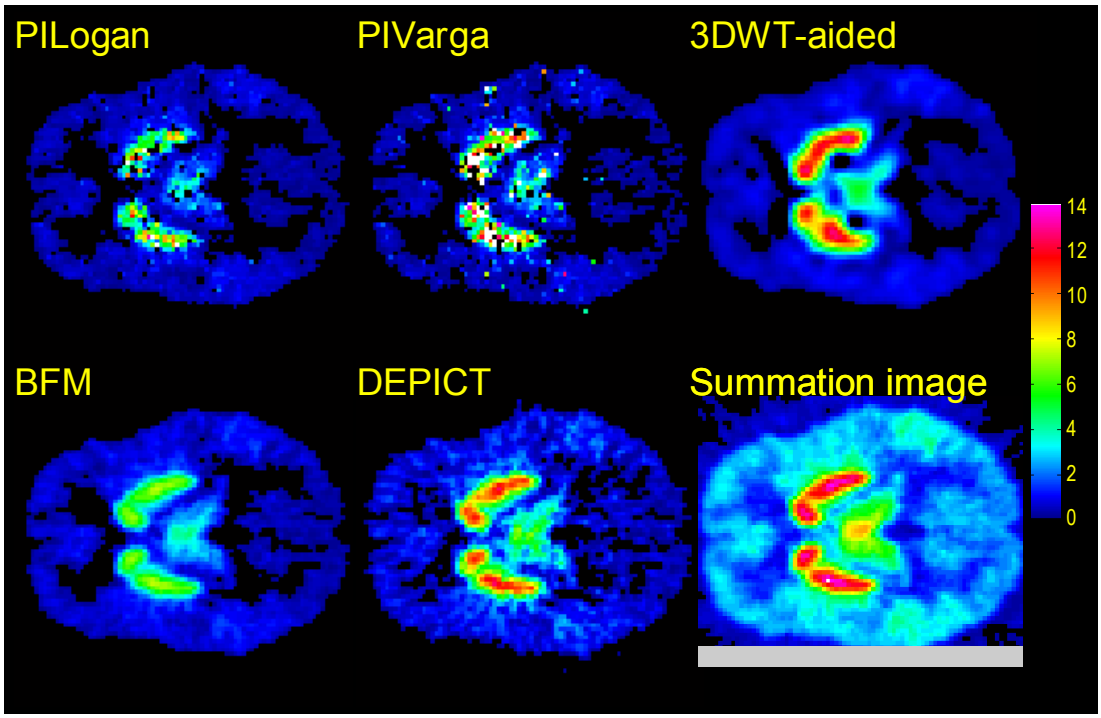

Figure 13

The BFM yielded a BP map with sharpness matching that of the summation image and the map had a noise-free appearance with smoothly varying estimated BP values (paper **II**). The BP estimated for low receptor density regions was overestimated, whereas it was underestimated for regions with high receptor density.

The BP map created by DEPICT was also sharp, noise-free and without outliers (paper **II**). However, areas of the image corresponding to lower receptor-density regions had a striped appearance similar to that of single time-frames of a 4-D PET image. BP obtained using the DEPICT approach was overestimated for all regions. For regions with low receptor density it was overestimated as much as about 175% of the reference values.

The 5-HT_{1A}-receptor BP maps created by the evaluated approaches had similar characteristics to the D_2/D_3 maps with regard to noisiness-smoothness, resolution etc (paper **II**). In contrast to the case of [^{11}C]FLB 457, the ratio of estimated BP values obtained with [^{11}C]WAY 100635 were in general more "stable", i.e. there was less variability across the target regions and smaller deviations from the reference values.

4.2 TESTING THE GANG MODEL

The results obtained on the first simulated dataset, in paper **III**, indicate that both the GNG and GANG model were able to map the topology and distribution of the input data. In case of the second dataset, the GNG model produced a network with the same number of units as in the first test. However, it failed to correctly map the topology of the data in the sparse, lower dimensional regions of the input. In contrast, the GANG model produced a network that maps the topology correctly even in the sparse (one-dimensional) regions. Figure 14 displays the mature GNG (14a) and GANG (14b) networks in the second test. The dashed lines indicate the outlines of the input dataset.

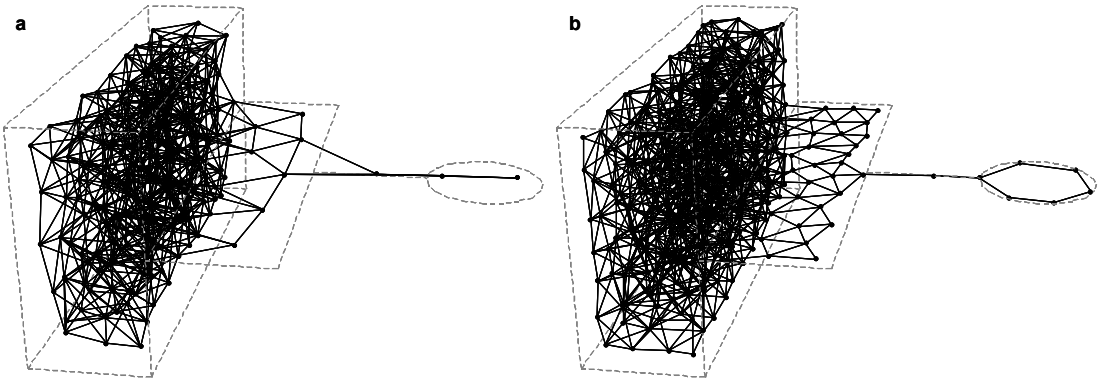

Figure 15

Training the GNG model on the simulated MR data resulted in a network with 225 units but with no units in the sparsest areas of feature space including the one corresponding to mild MS lesions. Therefore, after performing hierarchical clustering and image segmentation, no cluster could be picked as *the* "cluster of mild MS lesions", and input points from the MS lesion were classified to the closest clusters. Therefore, in an actual segmentation study this classification results in a large number of misclassified voxels. This is demonstrated in Figure 15d-f where all voxels belonging to the "cluster of MS lesions" are represented by white pixels. In short, the results of GNG-based multivariate segmentation cannot be easily used to detect early MS lesions.

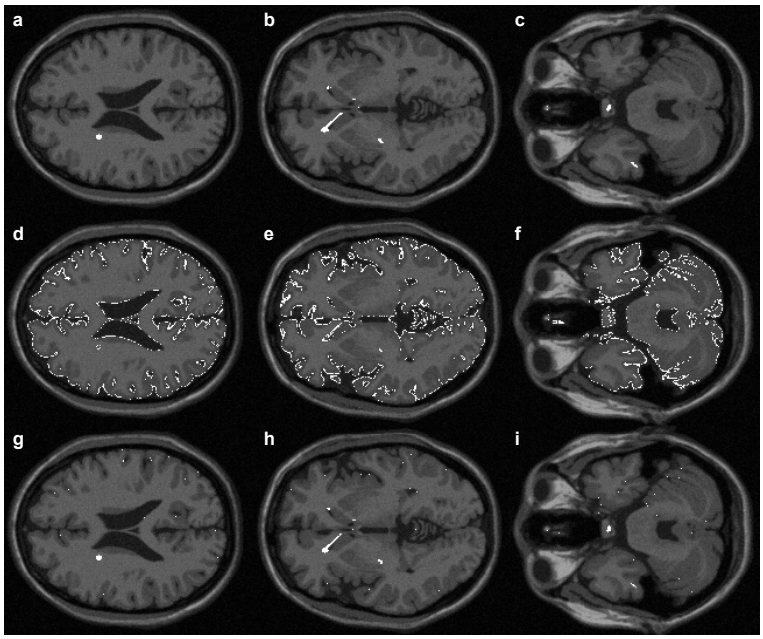

Figure 14

Training the GANG model with the multivariate MR dataset resulted in a network with 352 units. As described, units were grouped to clusters using hierarchical clustering. The units in the area of MS lesion points were assigned to a separate, distinct cluster. Figures 15g-i demonstrate the selection of this cluster as *the* "cluster of MS lesions". Voxels classified to this cluster include all MS lesions (see ground truth MS lesion voxels from the brain phantom in Figures 15a-c). Additional voxels were misclassified due to the noise present in the MR images. However, such voxels can probably be excluded using simple real space checks and/or using fuzzy cluster membership values. In short, the GANG technique was able to detect the presence of a small, extremely sparse region of the input dataset that, on the other hand, could have a high importance in case of an actual research study.

4.3 TESTING THE GANG BASED RECEPTOR PARAMETRIC MAPPING

The error goal of GANG training was optimised to yield 40-50 units (paper **IV**). The first analysis using the 16-dimensional feature space resulted in a GANG with 43 units. The second analysis using the two-dimensional feature space resulted in 44 units. The input datasets were classified using the final, mature GANG networks. Clusters (neighbourhoods) corresponding to the striatum had around 100 member points or even fewer in case of the second analysis. Extrastriatal regions, on the other hand, corresponded to neighbourhoods with several thousand points.

The voxels TAC's corresponding to points in the same neighbourhood were averaged to create "denoised" TAC's. Figures 16a and 16b display the average TAC's for the first and second analysis, respectively. The curves had been sorted for display according to their AUC values. Both analyses resulted in average TAC's with greatly reduced noise. The extrastriatal curves from the first analysis still contain some noise, mainly in the early time-frames. Otherwise, the curves reach the smoothness of TAC's from a ROI-based analysis.

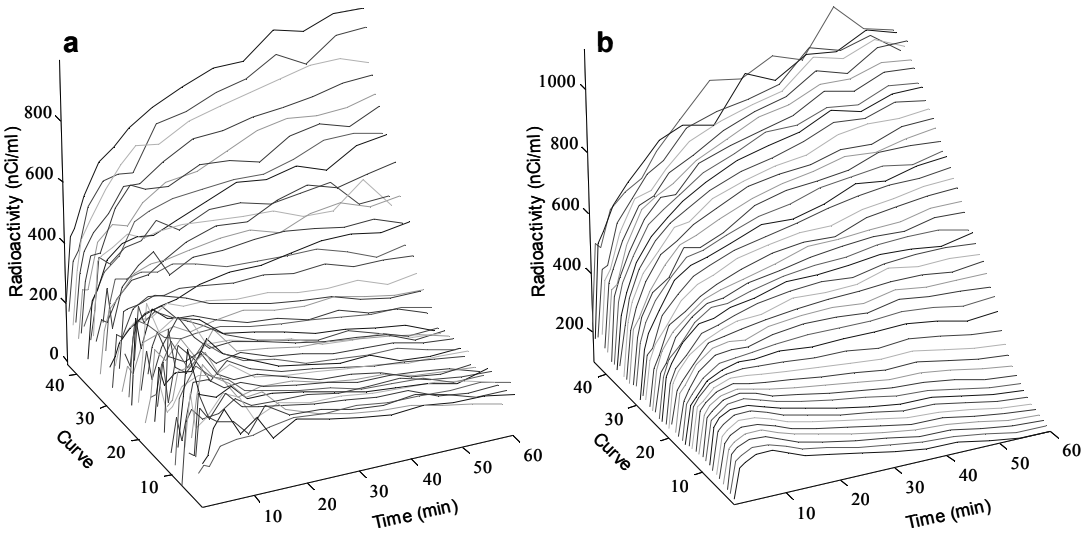

Figure 16

There was a good agreement between the estimated BP maps and between the maps and previous data on dopamine D_2 receptor studies with regard to the overall pattern of receptor distribution (Olsson et al., 1999)(also papers **I** and **II**). Furthermore, BP maps

from the same approach in the two analyses had very similar BP values but the BP maps in the second analysis had a smoother appearance. The lowest extrastriatal values were provided by the RLogan approach, whereas the highest by the PITCM approach. The BFM, SRTM and DEPICT approaches provided similar extrastriatal values. The LSRTM approach in the second analysis yielded extrastriatal values also similar to these three approaches. In the first analysis, however, the values were somewhat lower though still surpassing the results of the RLogan approach. The estimated striatal BP values were highest for the BFM and SRTM approaches in both analyses, followed by the PITCM, LSRTM, DEPICT and RLogan approaches in decreasing rank order.

The PICTM approach was the most complicated one in terms of using plasma TAC for input function and providing the broadest spectrum of parameters. The patterns of distribution for each parameter were similar between the corresponding maps of the two analyses. However, the voxel values had some discrepancies with generally higher estimated values in the first analysis. The most difference could be seen in the k_1 and k_2 maps. The k_3 and k_4 maps had fewer voxels with notable difference. The DVT maps were different mainly in the striatal and thalamic regions. The parametric values obtained were in good agreement visually with previously published results, especially in the second analysis (Olsson et al., 1999). Figure 17 displays the parametric maps obtained using the PITCM approach in the second analysis.

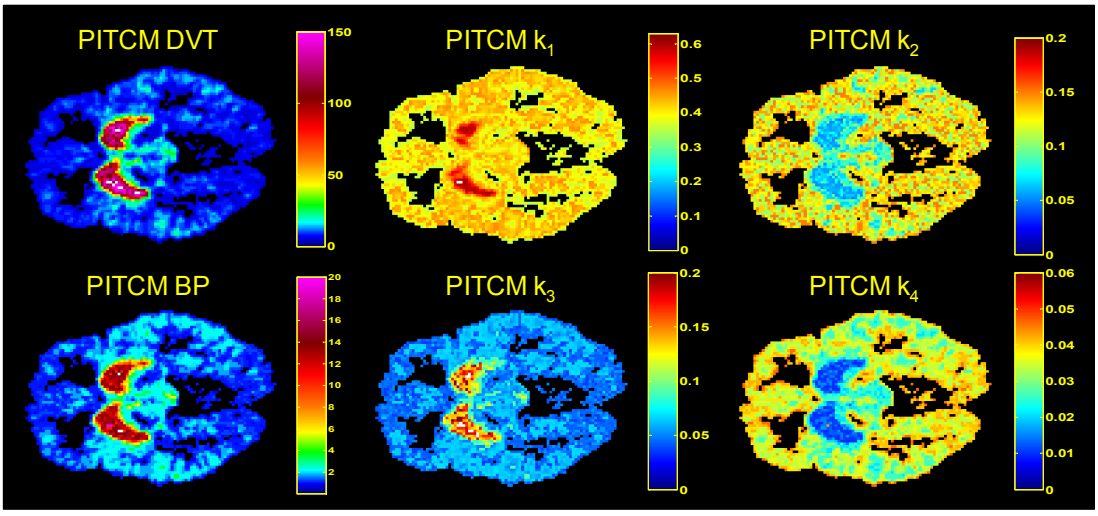

Figure 17

4.4 TESTING THE GANG BASED MULTI-RECEPTOR MAPPING

Figure 18a displays the input data in feature space (paper **V**). The 5-HT_{1A} receptor BP values display a greater spread, whereas 5-HT_1 transporter BP values are more packed. Negative values are present in the plot because many voxels are devoid of receptor in one or more of the subjects but still have a positive BP value in at least one of them.

The trained GANG created a total of 235 neighbourhoods in feature space, shown also in Figure 18a by shading input points in feature space according to their classification to neighbourhoods. The denser areas of the feature space have smaller neighbourhoods and vice versa.

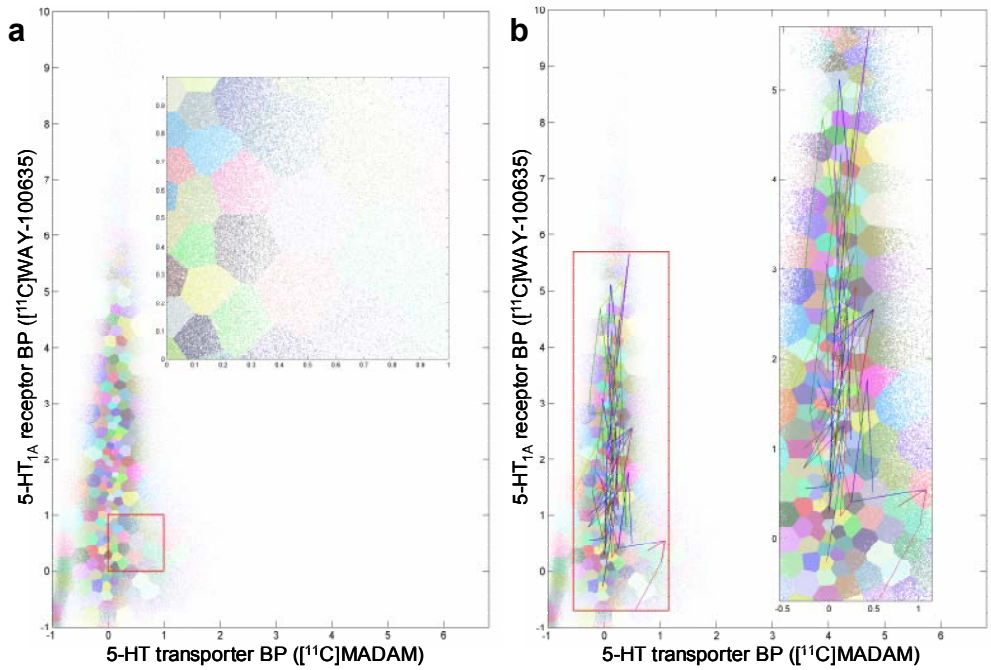

Figure 18

Figure 18b presents a few of the many thousand trajectories that were enumerated in the analysis. As shown in the figure, some voxels have a feature vector (and thus a multi-receptor pattern) moving intensively between individuals. On the other hand, some voxels display a more stable behaviour. For example the trajectory in the lower right corner is limited to three adjacent neighbourhoods in possibly four out of the five subjects.

After trajectory classification various trajectory metrics were obtained. Figure 19 displays sagittal cross sections through the map of trajectory classification and some final multi-receptor maps.

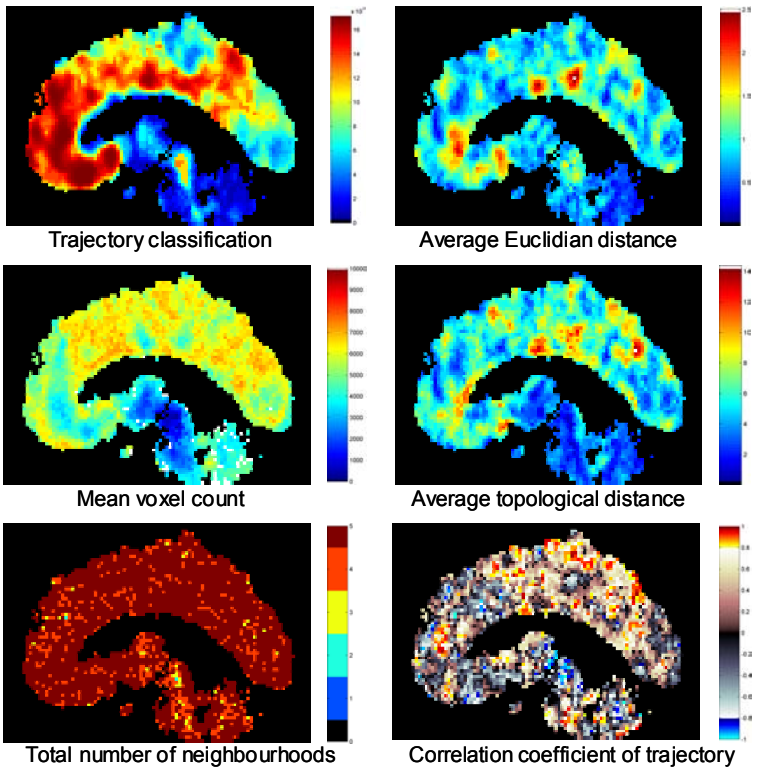

Figure 19

According to the mean voxel count and mean neighbourhood density metrics, the thalamus and the brain stem contained voxels in rather desolated, sparse neighbourhoods of the feature space. Also voxels in the frontal lobe and especially the anterior cingulate gyrus belonged to low-count trajectories. The average topological distance metric roughly and by large correlated with the average Euclidian distance. However, in some locations, such as in the limbic cortex or the midbrain, the neighbourhood length was high but the Euclidian distance was low and *vice versa*. The former indicated that the trajectory "crossed over" territories of the feature space with many small neighbourhoods and the latter the other way around.

The correlation coefficient analysis of the pre- and postsynaptic BP values indicated that pre- and post-synaptic BP values, and possibly receptor densities also, were more tightly coupled in such parts of the brain as the precingulate frontal cortex (positive correlation) or the diamesencephalic border (negative correlation). Although on a non-significant level but the anterior frontal cortex seems to be more negatively correlated (or less correlated on the whole) than the parietooccipital cortex and the paracentral cortex.

5 SUMMARY OF FINDINGS

- The combination of three-dimensional spatial wavelet filtering with existing parameter estimation procedures enables us to obtain detailed maps of radioligand binding parameters.
- From a selection of recent parametric mapping approaches, the wavelet-based approach gave the most valid estimates across regions representing a wide range of receptor densities in case of PET measurements obtained using [^{11}C]FLB 457 and [^{11}C]WAY100635.
- The field of parametric neuroreceptor imaging has reached a level of maturity for using the methods in applied studies.
- The growing adaptive neural gas artificial neural network model is able to adaptively map the distribution of the input data, including both dense and sparse regions, while detecting its local dimensionality, topology and radial dispersion. Therefore it can be applied, among others, in multi-modal or multi-recording cluster analysis, anatomical pattern recognition, image processing frameworks (e.g. image segmentation), or data mining.
- The approach of GANG based classification of voxel TAC's is a promising way to create noise-reduced or even noise-free input for estimating binding parameters and obtaining parametric maps with an arbitrary parameter estimation method.
- GANG based multi-receptor mapping can reveal complex relationships and inter-individual or inter-condition tendencies related to several receptor systems. An existing research interest of this kind is the study of pre- and post-synaptic receptors or transporter–receptor systems, such as 5-HT transporters and 5-HT$_{1A}$ receptors.

6 FUTURE RESEARCH

On-going work related to first level neuroreceptor studies applies the wavelet-based parametric mapping approach for the analysis of a large dataset obtained using dopamine D_2/D_3 radioligands [^{11}C]FLB 457 and [^{11}C]raclopride. The created BP maps are used in statistical analysis to reveal differences in dopaminergic receptor availability between groups of healthy and diseased subjects. This is a major step forward from performing group comparisons on regional averages.

The GANG-based noise reduction and parametric mapping framework is going to be evaluated for validity and reliability in cross-evaluations with traditional ROI-based and parametric mapping approaches. In parallel to this evaluation, another study is under preparation on the applicability of this approach for obtaining maps of absolute quantified receptor density (B_{max}) from several PET examinations of the same subject with different specific radioactivity of the radioligand.

The first application of the GANG-based multi-receptor mapping approach is going to be the study of relationships between sub-systems of the same neuroreceptor type such as 5-HT_{1A} receptors and 5-HT transporters. This was the model system used to demonstrate the capabilities of the approach but the actual applied study will require larger number of subjects so that reliable statistics can be obtained.

A third level and the pinnacle of neuroreceptor studies can be the construction of models describing physiological and/or pathological processes underpinning the patterns emerging from the second level of studies. This high level modelling has to encompass information on a broad spectrum of genetic and environmental factors. Therefore, it has to be based on a meta-analysis of results from several studies of different kind besides the results from first and second level neuroreceptor studies. The third level models, albeit possibly based on mathematically clear analytical models, can be expected to be computational models that seek to simulate certain aspects of the CNS within an artificial network. Such models have already been used to duplicate properties of physiological or pathological processes in the nervous system.

For example a computational model of motor circuitry in the lamprey spinal chord has been proposed that seeks to simulate network dynamics on a biophysical level (Hellgren et al., 1992; Lansner et al., 1998; Grillner, 2003). The model successfully reproduced physiological motor phenomena such as alternating phases of activity along the simulated spinal chord. Other computational models have been proposed for the study of certain phenomena of consciousness (Dehaene et al., 1987; Changeux and Dehaene, 1989, 2000; Dehaene and Changeux, 2000; Gisiger et al., 2000; Dehaene et al., 2003). These models reproduce network structure and dynamics of thalamic nuclei and cortical columns with thalamo-cortical, cortico-cortical connections. The models simulate membrane potential dynamics based on membrane, ion-channel and ionotropic receptor conductance. Simulation results could reproduce such patterns of neural activity as spontaneous thalamo-cortical oscillations, and conscious phenomena such as varying level of wakefulness or attentional blink.

Furthermore, models for CNS disease processes have also been proposed such as a computational model to explain different functional alterations in schizophrenia (Hoffman

and McGlashan, 2001; Siekmeier and Hoffman, 2002). The proposed models are based on observations from studies using a number of methodologies, ranging from simple histological staining, immunolabelling, cortical architectonics to neuroimaging methods as MRI diffusion tensor imaging or PET brain activation studies. In contrast to the biophysically detailed model used to simulate spinal chord motor circuits, these models capture network dynamics on a more abstract level. However, they have been successful in reproducing such pathological phenomena as spontaneous perception (hallucination) or enhanced semantic priming, or even in predicting results of functional performance tests.

Along these lines, the long-term objective of the research efforts should be the integration of knowledge acquired from first and second level studies with results of other investigations to create third level models on neuroreceptor systems and related physiological and pathological processes.

7 ACKNOWLEDGEMENTS

This thesis is the accomplishment of many years of doctoral studies through which I had the privilege to be supported, motivated and befriended by many the most talented and generous people. For this I am ceaselessly grateful and wish to explicitly thank the following:

Balázs Gulyás – my main supervisor who took the burden upon him of guiding, teaching and supporting me as a doctoral student even before I had received my medical diploma. For friendship, infecting with perpetual enthusiasm for research, sharing his ideas coming from an inexhaustible source of creativity and setting an example of being Magyar.

Professor Lars Farde – my co-supervisor who found place in his ever overcrowded schedule for teaching me the basic and advanced aspects of scientific thinking and writing. For being not just friendly but a friend ever since we spun around in a car of the Hungarian Ministry of Domestic Affairs in Budapest, for showing how the best "codec" for scientific communication works during many hours of "mangla" sessions.

Professor Christer Halldin – whom I also had the honour of getting acquainted with during that winter long time ago in Budapest. For providing economic, infrastructural and many other important conditions for my thesis research, for being ever-patient in explaining me various topics including even the most basic administrative issues.

Both Lars and Christer – for letting me share with them the delicacies of the *vinum regum*, *rex vinorum*, for sharing several good times at "Fekete holló" with showing their genuine love for Hungarian cuisine and gipsy music.

Docent Anna-Lena Nordström – for kindly providing help even amongst great loads of work.

Docent Håkan Hall – who was my first tutor before I came over to *in vivo* research. For implanting the enthusiasm for studying the receptors of the human brain, for teaching me the mastery of autoradiography and fundamentals of ligand-receptor binding, for sharing good hours in Debrecen and Stockholm.

Assistant Siv Eriksson – for not only letting me learn from her the practicalities of whole human hemisphere sectioning and autoradiography but also showing that her name "Siv" truly means a warm "Szív".

Research-nurse Kjerstin Lind – for being a tireless helper with practical problems related to my research, for having many cheerful talks, for bringing dedicated samples to me from their delicious home made apple juice, the best of Sweden.

Dr. Hans Olsson – my friend and student-fellow. For innumerable brainstorming sessions that always lead to new inspirations, ideas tremendously contributing to finding paths to follow during my research, for being there to discuss any matter of unimportance or importance outside research (such as the "mountains of Debrecen" or "The Meaning of Life") with life-elongatingly good laughs.

Dr. Per Karlsson – for having good talks on issues from setting up the imaging database to gracefulness of the Mac, for being always eager to help.

Dr. Stefan Pauli – for his incredible enthusiasm and capacity to discuss, at any time, any major to minute detail of anything that is related to any physical or computational aspect of neuroreceptor imaging or anything else that is of concern to his talking peer.

Dr. Bengt Andrée, Dr. Nina Erixon, Dr. Judit Sóvágó, Dr. Johan Lundberg, Dr. Simon Cervenka, Dr. Aurelia Jucaite, Dr. Mirjam Talvik, psychologist Jacqueline Borg – for having many good discussions and laughs and giving help when needed.

Ulla-Kajsa Pehrsson, Marianne Youssefi, – for patiently and kindly helping me with any administrative task as well as for refreshing talks.

Göran Rosenqvist, Urban Hansson – the wizards whom one can count on.

Dr. Géza Szilágyi and his Ági, Dr. Szabolcs Kéri and his Helga – outside colleagues and friends from Hungary. For giving good company and stimulating discussions.

My parents István and Magdolna – for their love and for always supporting me in my pursuits in many, many ways.

My brother István – for first motivating me to come to Sweden, for setting an example to follow, for being always there to help with his wife Györgyi and kids Bence and Bella.

Finally, I thank you, Veronika, breath of fresh air for my soul, for your love, understanding as well as for your companionship and support.

8 REFERENCES

BrainWeb: Simulated Brain Database. URL: http://www.bic.mni.mcgill.ca/brainweb/.

Aldenderfer, M.S., Blashfield, R.K., 1984. Cluster analysis, Sage Publications, Newbury Park, California.

Andree, B., Halldin, C., Thorberg, S.O., Sandell, J., Farde, L., 2000. Use of PET and the radioligand [carbonyl-(11)C]WAY-100635 in psychotropic drug development. Nucl Med Biol 27, 515-521.

Ashburner, J., Haslam, J., Taylor, C., Cunningham, V.J., Jones, T., 1996. A cluster analysis for the characterisation of dynamic PET data. In: Myers R., Cunningham V.J., Bailey D., Jones T. (Eds.), Quantification of Brain Function Using PET, Academic Press, San Diego, CA, pp. 301-306.

Battle, G., 1987. A block spin construction of ondolettes. Part I: Lemarie functions. Commun Math Phys 110, 601-615.

Bergstrom, M., Boethius, J., Eriksson, L., Greitz, T., Ribbe, T., Widen, L., 1981. Head fixation device for reproducible position alignment in transmission CT and positron emission tomography. J Comput Assist Tomogr 5, 136-141.

Bracewell, R., 2004. Fourier Analysis and Imaging, Plenum Press US, New York.

Carson, R.E., Daube-Witherspoon, M.E., Herscovitch, P., (Eds.), 1998. Quantitative functional brain imaging with positron emission tomography, Academic Press, San Diego.

Chalon, S., Tarkiainen, J., Garreau, L., Hall, H., Emond, P., Vercouillie, J., Farde, L., Dasse, P., Varnas, K., Besnard, J.C., Halldin, C., Guilloteau, D., 2003. Pharmacological characterization of N,N-dimethyl-2-(2-amino-4-methylphenyl thio)benzylamine as a ligand of the serotonin transporter with high affinity and selectivity. J Pharmacol Exp Ther 304, 81-87.

Changeux, J.P., Dehaene, S., 1989. Neuronal models of cognitive functions. Cognition 33, 63-109.

Changeux, J.P., Dehaene, S., 2000. Hierarchical neuronal modeling of cognitive functions: from synaptic transmission to the Tower of London. Int J Psychophysiol 35, 179-187.

Cocosco, C.A., Kollokian, V., Kwan, R.K.-S., Evans, A.C., 1997. BrainWeb: Online interface to a 3D MRI simulated brain database. In: Proceedings of 3rd International Conference on Functional Mapping of the Human Brain, Coppenhagen, Denmark. pp. S425.

Collins, D.L., Zijdenbos, A.P., Kollokian, V., Sled, J.G., Kabani, N.J., Holmes, C.J., Evans, A.C., 1998. Design and construction of a realistic digital brain phantom. IEEE Trans Med Imaging 17, 463-468.

Cooper, J.R., Bloom, F.E., Roth, R.H., 2002. The Biochemical Basis of Neuropharmacology, University Press, Oxford.

Daszykowski, M., Walczak, B., Massart, D.L., 2002. On the optimal partitioning of data with K-means, Growing K-means, Neural Gas, and Growing Neural Gas. J Chem Inf Comput Sci 42, 1378-1389.

Daubechies, I., 1992. Ten lectures on wavelets, PA: Society for Industrial and Applied Mathematics, Philadelphia.

Dehaene, S., Changeux, J.P., 2000. Reward-dependent learning in neuronal networks for planning and decision making. Prog Brain Res 126, 217-229.

Dehaene, S., Changeux, J.P., Nadal, J.P., 1987. Neural networks that learn temporal sequences by selection. Proc Natl Acad Sci U S A 84, 2727-2731.

Dehaene, S., Sergent, C., Changeux, J.P., 2003. A neuronal network model linking subjective reports and objective physiological data during conscious perception. Proc Natl Acad Sci U S A 100, 8520-8525.

Delforge, J., Bottlaender, M., Loc'h, C., Guenther, I., Fuseau, C., Bendriem, B., Syrota, A., Maziere, B., 1999. Quantitation of extrastriatal D2 receptors using a very high-affinity ligand (FLB 457) and the multi-injection approach. J Cereb Blood Flow Metab 19, 533-546.

Dittenbach, M., Merkl, D., Rauber, A., 2001. Hierarchical clustering of document archives with the Growing Hierarchical Self-Organizing Map. In: Proceedings of ICANN01 International Conference on Artificial Neural Networks, Springer-Verlag London, UK Vienna, Austria. pp. 500-508.

Drevets, W.C., Frank, E., Price, J.C., Kupfer, D.J., Holt, D., Greer, P.J., Huang, Y., Gautier, C., Mathis, C., 1999. PET imaging of serotonin 1A receptor binding in depression. Biol Psychiatry 46, 1375-1387.

English, R.J., Brown, S.E., 1990. SPECT: Single-Photon Emission Computed Tomography : A Primer, Society of Nuclear Medicine, Reston.

Everitt, B.S., Landau, S., Leese, M., 2001. Cluster Analysis, Arnold Publishers, London.

Farde, L., Ito, H., Swahn, C.G., Pike, V.W., Halldin, C., 1998. Quantitative analyses of carbonyl-carbon-11-WAY-100635 binding to central 5-hydroxytryptamine-1A receptors in man. J Nucl Med 39, 1965-1971.

Farde, L., Suhara, T., Nyberg, S., Karlsson, P., Nakashima, Y., Hietala, J., Halldin, C., 1997. A PET-study of [11C]FLB 457 binding to extrastriatal D2-dopamine receptors in healthy subjects and antipsychotic drug-treated patients. Psychopharmacology (Berl) 133, 396-404.

Firenze, F., Morasso, P., 1994. Adaptive modulation of receptive fields in self-organizing networks. In, International Conference on Artificial Neural Networks, Springer-Verlag, London.

Firenze, F., Schenone, A., Sormani, M.P., Lanza, P., 1994. A self-organizing network applied to segmentation of multimodal biomedical images. In: Proceedings of ICANN94 International Conference on Artificial Neural Networks, Sorrento.

Flexer, A., 2001. On the use of self-organizing maps for clustering and visualization. Intell Data Anal 5, 373-384.

Frank, G.K., Kaye, W.H., Meltzer, C.C., Price, J.C., Greer, P., McConaha, C., Skovira, K., 2002. Reduced 5-HT2A receptor binding after recovery from anorexia nervosa. Biol Psychiatry 52, 896-906.

Fritzke, B., 1994. Growing cell structures - a self-organizing network for unsupervised and supervised learning. Neural Networks 7, 1441-1460.

Fritzke, B., 1995. A Growing Neural Gas Network Learns Topologies. In: Tesauro G., Touretzky D.S., Leen T.K. (Eds.), Advances in Neural Information Processing Systems 7, MIT Press, Cambridge MA, pp. 625-632.

Georges-Schleuter, M., 1992. Comparison of local mating strategies in massively perellel genetic algorithms. In: Männer R., Manderick B. (Eds.), Parallel problem solving from nature 2, North-Holland, Amsterdam.

Gisiger, T., Dehaene, S., Changeux, J.P., 2000. Computational models of association cortex. Curr Opin Neurobiol 10, 250-259.

Goldberg, D.E., 1989. Genetic algorithms in search, optimization and machine learning, Addison Wesley Publishing Company, Reading, MA, USA.

Grillner, S., 2003. The motor infrastructure: from ion channels to neuronal networks. Nat Rev Neurosci 4, 573-586.

Gunn, R.N., Gunn, S.R., Turkheimer, F.E., Aston, J.A., Cunningham, V.J., 2002. Positron emission tomography compartmental models: a basis pursuit strategy for kinetic modeling. J Cereb Blood Flow Metab 22, 1425-1439.

Gunn, R.N., Lammertsma, A.A., Hume, S.P., Cunningham, V.J., 1997. Parametric imaging of ligand-receptor binding in PET using a simplified reference region model. Neuroimage 6, 279-287.

Guo, H., Renaut, R., Chen, K., Reiman, E., 2003. Clustering huge data sets for parametric PET imaging. Biosystems 71, 81-92.

Halldin, C., Farde, L., Hogberg, T., Mohell, N., Hall, H., Suhara, T., Karlsson, P., Nakashima, Y., Swahn, C.G., 1995. Carbon-11-FLB 457: a radioligand for extrastriatal D2 dopamine receptors. J Nucl Med 36, 1275-1281.

Hellgren, J., Grillner, S., Lansner, A., 1992. Computer simulation of the segmental neural network generating locomotion in lamprey by using populations of network interneurons. Biol Cybern 68, 1-13.

Hoffman, R.E., McGlashan, T.H., 2001. Neural network models of schizophrenia. Neuroscientist 7, 441-454.

Kessler, R.M., Whetsell, W.O., Ansari, M.S., Votaw, J.R., de Paulis, T., Clanton, J.A., Schmidt, D.E., Mason, N.S., Manning, R.G., 1993. Identification of extrastriatal dopamine D2 receptors in post mortem human brain with [125I]epidepride. Brain Res 609, 237-243.

Kiang, M.Y., 2001. Extending the Kohonen self-organizing map networks for clustering analysis. Comput Stat Data An 38, 161-180.

Kimura, Y., 2004. Formation of parametric images with statistical clustering. International Congress Series 1265, 25-30.

Kimura, Y., Hsu, H., Toyama, H., Senda, M., Alpert, N.M., 1999. Improved signal-to-noise ratio in parametric images by cluster analysis. Neuroimage 9, 554-561.

Kimura, Y., Senda, M., Alpert, N.M., 2002. Fast formation of statistically reliable FDG parametric images based on clustering and principal components. Phys Med Biol 47, 455-468.

Kwan, R.K., Evans, A.C., Pike, G.B., 1999. MRI simulation-based evaluation of image-processing and classification methods. IEEE Trans Med Imaging 18, 1085-1097.

Lam, S., Shen, Y., Nguyen, T., Messier, T.L., Brann, M., Comings, D., George, S.R., O'Dowd, B.F., 1996. A serotonin receptor gene (5HT1A) variant found in a Tourette's syndrome patient. Biochem Biophys Res Commun 219, 853-858.

Lammertsma, A.A., Hume, S.P., 1996. Simplified reference tissue model for PET receptor studies. Neuroimage 4, 153-158.

Lansner, A., Kotaleski, J.H., Grillner, S., 1998. Modeling of the spinal neuronal circuitry underlying locomotion in a lower vertebrate. Ann N Y Acad Sci 860, 239-249.

Lemarie, P.G., 1988. Ondolettes a localization exponentielles. J Math Pures et Appl 67, 227-236.

Liptrot, M., Adams, K.H., Martiny, L., Pinborg, L.H., Lonsdale, M.N., Olsen, N.V., Holm, S., Svarer, C., Knudsen, G.M., 2004. Cluster analysis in kinetic modelling of the brain: a noninvasive alternative to arterial sampling. Neuroimage 21, 483-493.

Logan, J., Fowler, J.S., Volkow, N.D., Ding, Y.S., Wang, G.J., Alexoff, D.L., 2001. A strategy for removing the bias in the graphical analysis method. J Cereb Blood Flow Metab 21, 307-320.

Logan, J., Fowler, J.S., Volkow, N.D., Wang, G.J., Ding, Y.S., Alexoff, D.L., 1996. Distribution volume ratios without blood sampling from graphical analysis of PET data. J Cereb Blood Flow Metab 16, 834-840.

Logan, J., Fowler, J.S., Volkow, N.D., Wolf, A.P., Dewey, S.L., Schlyer, D.J., MacGregor, R.R., Hitzemann, R., Bendriem, B., Gatley, S.J., et al., 1990. Graphical analysis of reversible radioligand binding from time-activity measurements applied to [N-11C-methyl]-(-)-cocaine PET studies in human subjects. J Cereb Blood Flow Metab 10, 740-747.

Mallat, S.G., 1989. A theory of multiresolution signal decomposition: the wavelet representation. IEEE Trans Pattern Anal Machine Intell 11, 673-693.

Martinetz, T.M., 1993. Competitive Hebbian learning rule forms perfectly topology preserving maps. In, ICANN'93: International Conference on Artificial Neural Networks, Springer, Amsterdam, pp. 427-434.

Meyer, Y., 1992. Wavelets and operators, Cambridge University Press.

Moresco, F.M., Dieci, M., Vita, A., Messa, C., Gobbo, C., Galli, L., Rizzo, G., Panzacchi, A., De Peri, L., Invernizzi, G., Fazio, F., 2002. In vivo serotonin 5HT(2A) receptor binding and personality traits in healthy subjects: a positron emission tomography study. Neuroimage 17, 1470-1478.

Mühlenbein, H., Schomisch, M., Born, J., 1991. The parallel genetic algorithm as a function optimizer. Parallel Computing 17, 619-632.

Olsson, H., Halldin, C., Swahn, C.G., Farde, L., 1999. Quantification of [11C]FLB 457 binding to extrastriatal dopamine receptors in the human brain. J Cereb Blood Flow Metab 19, 1164-1173.

Roland, P.E., Graufelds, C.J., Wåhlin, J., Ingelman, L., Andersson, M., Ledberg, A., Pedersen, J., Åkerman, S., Dabringhaus, A., Zilles, K., 1994. Human brain atlas: For high-resolution functional and anatomical mapping. Hum Brain Map 1, 173-184.

Romesburg, C., 2004. Cluster Analysis for Researchers, Lulu Press, North Carolina.

Sandberg, I.W., 1978. On the mathematical foundations of compartmental analysis in biology, medicine, and ecology. IEEE Trans Circuits Syst CAS 25, 273-279.

Schenone, A., Firenze, F., Acquarone, F., Gambaro, M., Masulli, F., Andreucci, L., 1996. Segmentation of multivariate medical images via unsupervised clustering with "adaptive resolution". Comput Med Imaging Graph 20, 119-129.

Siegel, G.J., Albers, R.W., Agranoff, B.W., Fisher, S.K., Uhler, M.D., 1999. Basic Neurochemistry: Molecular, Cellular and Medical Aspects, Lippincott Williams & Wilkins Publishers.

Siekmeier, P.J., Hoffman, R.E., 2002. Enhanced semantic priming in schizophrenia: a computer model based on excessive pruning of local connections in association cortex. Br J Psychiatry 180, 345-350.

Suhara, T., Sudo, Y., Okauchi, T., Maeda, J., Kawabe, K., Suzuki, K., Okubo, Y., Nakashima, Y., Ito, H., Tanada, S., Halldin, C., Farde, L., 1999. Extrastriatal dopamine D2 receptor density and affinity in the human brain measured by 3D PET. Int J Neuropsychopharmcol 2, 73-82.

Turkheimer, F.E., Banati, R.B., Visvikis, D., Aston, J.A., Gunn, R.N., Cunningham, V.J., 2000. Modeling dynamic PET-SPECT studies in the wavelet domain. J Cereb Blood Flow Metab 20, 879-893.

Turkheimer, F.E., Brett, M., Aston, J.A., Leff, A.P., Sargent, P.A., Wise, R.J., Grasby, P.M., Cunningham, V.J., 2000. Statistical modeling of positron emission tomography images in wavelet space. J Cereb Blood Flow Metab 20, 1610-1618.

Turkheimer, F.E., Brett, M., Visvikis, D., Cunningham, V.J., 1999. Multiresolution analysis of emission tomography images in the wavelet domain. J Cereb Blood Flow Metab 19, 1189-1208.

Unser, M., Thevenaz, P., Lee, C., Ruttiman, U.E., 1995. Registration and statistical analysis of PET images using the wavelet transform. IEEE Eng Med Biol Mag 14, 603-611.

Verhoeff, N.P., 1993. Neuroreceptor ligand imaging by single photon emission comoputerised tomography (SPECT), Rodopi, Amsterdam.

Verhoeff, N.P., Meyer, J.H., Kecojevic, A., Hussey, D., Lewis, R., Tauscher, J., Zipursky, R.B., Kapur, S., 2000. A voxel-by-voxel analysis of [18F]setoperone PET data shows no substantial serotonin 5-HT(2A) receptor changes in schizophrenia. Psychiatry Res 99, 123-135.

Vesanto, J., Alhoniemi, E., 2000. Clustering of the self-organizing map. IEEE T Neural Networ 11, 586-600.

von Spiczak, S., Whone, A.L., Hammers, A., Asselin, M.C., Turkheimer, F., Tings, T., Happe, S., Paulus, W., Trenkwalder, C., Brooks, D.J., 2005. The role of opioids in restless legs syndrome: an [11C]diprenorphine PET study. Brain.

Wienhard, K., Dahlbom, M., Eriksson, L., Michel, C., Bruckbauer, T., Pietrzyk, U., Heiss, W.D., 1994. The ECAT EXACT HR: performance of a new high resolution positron scanner. J Comput Assist Tomogr 18, 110-118.

Wong, K.P., Feng, D., Meikle, S.R., Fulham, M.J., 2002. Segmentation of dynamic PET images using cluster analysis. IEEE Trans Nucl Sci 49, 200-207.

Zhou, Y., Huang, S.C., Bergsneider, M., Wong, D.F., 2002. Improved parametric image generation using spatial-temporal analysis of dynamic PET studies. Neuroimage 15, 697-707.